공학박사 학위논문

Surface and Structural Engineering of Ionovoltaic Device for Energy Harvesting and Sensing Applications

에너지 수확과 센서 활용을 위한 ionovoltaic 장치의 표면 개질과 구조 공정에 관한 연구

2019년 2월

서울대학교 융합과학기술대학원

나노융합학과 나노융합전공

양 영 준

Surface and Structural Engineering of Ionovoltaic Device for Energy Harvesting and Sensing Applications

지도교수 김 연 상

이 논문을 공학박사학위 논문으로 제출함.

2019년 2월

서울대학교 융합과학기술대학원
나노융합학과 나노융합전공

양 영 준

양영준의 박사학위 논문을 인준함

2019 년 1 월

위 원 장	박 원 철	인
부위원장	김 연 상	인
위 원	이 강 원	인
위 원	신 채 호	인
위 원	한 철 종	인

Abstract

Surface and Structural Engineering of Ionovoltaic Device for Energy Harvesting and Sensing Applications

YoungJun Yang

Program in Nano Science and Technology

The Graduate School of Convergence Science & Technology

Seoul National University

Recently, there has been a lot of interest in the research on the transducers using the phenomenon of electricity generation in the contact between the liquid and solid surface. In particular, transducers using EDL (electrical double layer) modulations, which named as ionovoltaic transducers are attracting attention because of their advantages in eco-friendly, simple drive systems and self-powered characteristics. With the growing need for renewable and eco-friendly energy generation devices and the increasing demand for a variety of sensors that can actively operate on an aqueous

solution basis, the ionovoltaic devices can be utilized as a great candidate to solve these demands. However, the output energy density is low and the fabrication process is complicated to make practical use of the ionovoltaic device as the energy generating device and the active sensors. Moreover, the driving principle of the device which is not sufficiently clarified and the similar materials and structures research of the device are obstructing the various utilization development of the device. In this thesis clarifies the generation of electricity by the ionic behavior at the interface through two issues: (i) surface modification of ionovoltaic device and (ii) improvement of ionovoltaic device performance through the structural engineering. In addition, this study covers a wide range of applications as sensors and energy harvesting devices.

First, applying a hydrophobic surface modification with novel electrical properties to the ionovoltaic device by engineering the hydrophobic layer, and applying it to various sensing applications using ionic behaviors at the solid-liquid interface. The ionovoltaic transducers with a negative / a positive surface potentials were developed and compared, and the effect of reversing the electrical signal by ionic behavior was confirmed for the first time. In addition, the modified ionovoltaic transducer has proven its applicability as a pH sensor and urea (bio)sensor by utilizing a pH-sensitive surface.

Secondly, we identified the principle that the contact between the liquid and the solid

surface is converted into the electric signal through the new type of device through the structural engineering and to apply it as the sensing and energy harvesting device. In addition, through electrode studies, we have understood the conduction mechanism and investigated the effect of resistance on ionovoltaic device performance. Through the whole structural engineering of the ionovoltaic device and the electrode modification, it was possible to control the generation time of the electric signal and to increase the energy density. Moreover, we have developed an energy harvester that can be used for the exterior and windows of buildings or automobiles through the development of high-resistance ITO mono- electrodes using the sputtering system, suggesting wide application possibilities of ionovoltaic devices.

Keywords: Ionovoltaic device, Solid-Liquid Interface, Sensor, Energy Harvester, Surface Modification, Structural Engineering

Student Number: 2013-23749

Contents

List of figures

Chapter 1

Chapter 2

Chapter 3

stage of the fabrication process. The XPS analysis data of the SP (b, d) and SAP devices (c, f) surfaces. The fluorine spectra and nitrogen spectra were analyzed for the SP and SAP active transducers.

Figure 3. 4(a) The peak voltage measured according to the change in the load resistance for the SP and SAP devices, and power levels obtained by calculations. (b) Measurement of the generated peak voltage by the ion concentration for both devices. (c) Measurement of the generated peak voltage in DI water and in the 10^{-3} M NaCl and MgCl2 solutions. In the experiments, 30 μL water droplets dropped from a height of 5 mm were used.

Figure 3. 5 Net surface potential variation of ionovoltaic device by the pH of solutions and ion dynamic at the solid-liquid interface.

Figure 3. 6 (a) Peak voltage measurement according to various pH levels for the SAP device. (b) Reproduction and reliability evaluation by alternately dropping acid (pH 3) and base (pH 11) droplets. Droplets at pH 7 were dropped between the dropping of acid and base water droplets. (c) Voltage measurement upon the dropping of acid water droplets immediately after the dropping of base water droplets.

Figure 3. 7 Fabrication method of the ionovoltaic urea biosensor and an AFM

image of the probe with urease. (A) The length and width of the transducer are 6 and 1 cm, respectively. The gap between the probe and the transducer is 0.3 cm. Three layers of urease-PEI were deposited onto a glass probe by the LBL method (enlarged image). (B) AFM image of the urease on the probe.

Figure 3. 8 Schematic images of the operating mechanism and measured surface zeta potential in acid and base conditions. (a) Operating condition and direction of the output current in an acid and a base. (b) Output voltage and schematic image of the surface in the acidic condition. (c) Output voltage and schematic image of the surface in the basic condition.

Figure 3. 9 Schematic images of the interface and measured surface zeta potential in acid and base conditions. (a) Schematic images of the surfaces in the acidic condition and (b) in the basic condition. (c) Measured OCV and surface zeta potential of the ionovoltaic transducer according to variations of the pH.

Figure 3. 10 Performance of the ionovoltaic urea sensor. (a) The measured output voltage with 10 mM of urea in the normal mode with the speed of the probe set to 6 cm/s. The output voltage was measured in all cases during backward/forward motions, and it can be divided into four regions.

(b) Enlarged data of the output voltage measured in the four sections. (c, d) Output voltages in the normal mode and expanded mode. In the data, only the output voltage during backward motion was extracted and normalized

Figure 3. 11 Measured output voltage (backward motion only) according to the urea concentration in the normal mode: (a) 50 mM, (b) 10 mM, (c) 5 mM, (d) 1 mM and (e) 0.5 mM.

Figure 3. 12 Measured inversion time according to the urea concentration. (a) VIT according to the urea concentration in the normal mode within the range of 50 mM to 1 mM. (b) VIT comparison in the normal and expanded modes with 10 and 50 mM of urea.

Figure 3. 13 Measured VIT according to the number of urease layers and reusability test results. (a) VIT measured by attaching urease-PEI layers from one layer to three layers to the probe. The VITs were measured in the normal mode with 10mM of urea. (b) A reusability test was carried out using three layers of urease-PEI with 10 mM of urea. The transducer and probe were washed with DI water and dried with N_2 gas after each test.

Figure 3. 14 Effects of voltage inversion for the ionovoltaic urea sensor with

into contact with the top and bottom electrodes (a). With the contact of the water and electrodes, the circuit is shorted, and EDLs are formed at the top and bottom electrodes (b). At that time, voltage difference follows the equation10 shown in (b), where RW and RL are the resistance of the water and circuit like the voltmeter and wires; Vt and Vb are the voltages on Ct and Cb. The bottom electrode effect is small enough to be negligible. Thus, the voltage difference can be expressed as the equation shown in (c).

Figure 4. 4 (a) shows the output power when multiple columns of water (10 cm) and air (30 cm) moved with a volumetric flow rate of 30 ml/min. Inset plot shows the generated energy per a cycle. (b) The measured peak to peak voltages and peak power averages at different volumetric flow rates. (c) The voltage data from a storage circuit (inset) containing a capacitor and a full wave rectifier.

Figure 4. 5 (a) shows application of the FEG for a segmented flow sensor with a two phase flow. (b), (c) High-speed camera images of the flowing water column from top view.

Figure 4. 6 (a) Schematic and photograph images of ITO mono-electrode based ionovoltaic device. (b) Output performance of the device (sample O4)

Chapter 1 Introduction

1.1 Overview

The ionovoltaic device that generates electricity using the movement of a water droplet on a certain solid surface, was developed and named by our research group in 2013. The device is capable of producing enough electricity to turn on a LED with a single droplet of water and has a high energy conversion efficiency of 28.9%. In addition, the ionovoltaic device can operate with various types of water motions, such as rain, vibration, and waves, so that the possibility of utilization is very high [1-8].

In the early stages of the ionovoltaic device study, the origin of electricity generation was studied [2-3]. Currently, various types of ionovoltaic devices have been developed that utilize the working principle of electricity generation from the contact of water droplets with certain solids for practical applications [1-8] [Fig. 1.1].

This device can be used as a good candidate to solve the need for renewable and eco-friendly energy due to environmental problems such as fine dust and greenhouse effect. In addition, we believe that the ionovoltaic device can be applied to the use of aqueous-based sensors in the Fourth Industrial Revolution

where the role of the sensor becomes more important.

This thesis deals with the applications of ionovoltaic device as an energy harvester and a sensor. For this purpose, we have explored and improved the characteristics of the device through surface modification and structural engineering of the device. Through this work, we could understand the driving principle more precisely and use a wide range of applications under various environment.

The working mechanism of the ionovoltaic device is identified and discussed on the components of the device, particularly the surface and structure through a review of previous studies in Chapter 2. In Chapter 3, we induced changes in ionic behaviors through surface modification of the ionovoltaic device and verified the applicability of the pH sensor and urea sensor by utilizing the unique electrical characteristics of the device. In Chapter 4, the relationship between the resistance and the performance of the device is investigated through the structural engineering and electrode modification of the device. In addition, the utilization of the ionovoltaic device as an energy harvester and sensor is introduced. Finally, Chapter 5 discusses the future direction of the ionovoltaic device through the identification of its advantages and disadvantages, together with the comprehensive conclusion of this study.

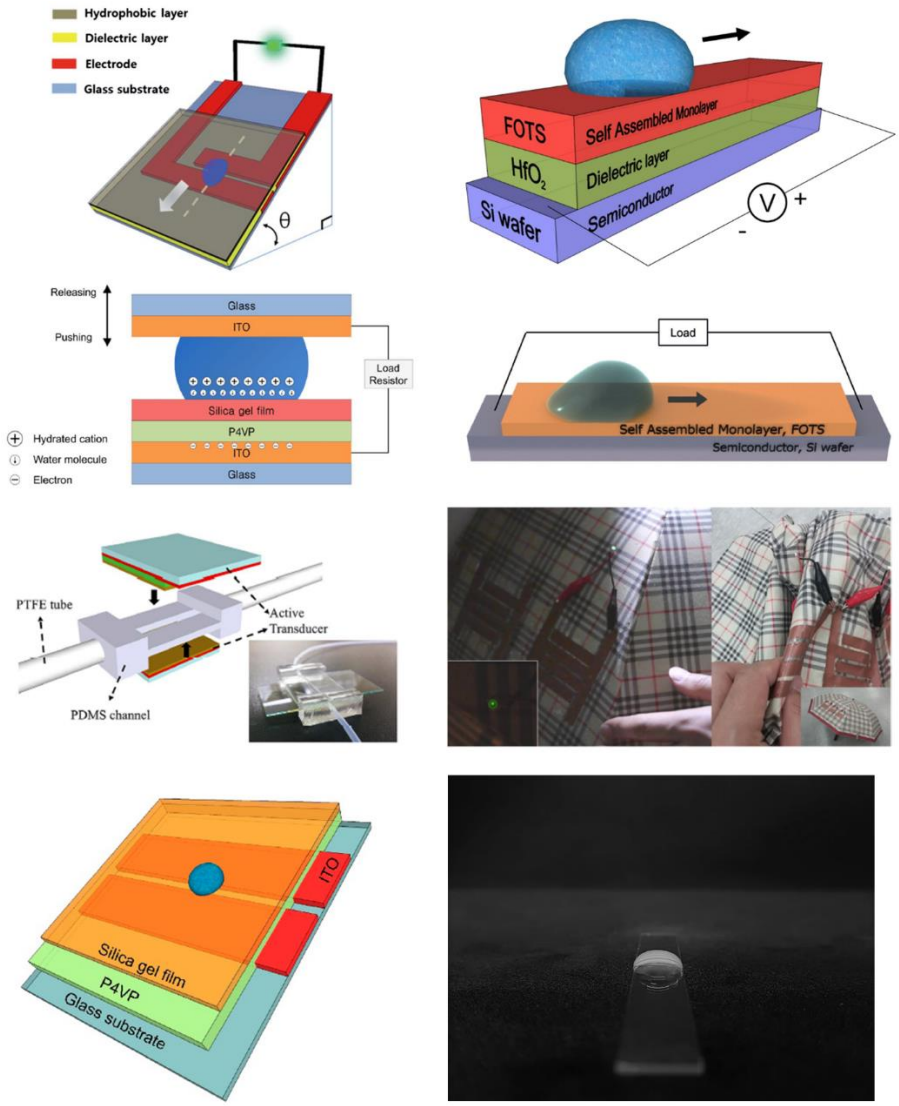

Figure 1. 1 . Schematic and photograph images of various ionovoltaic devices [1-8].

1.2 Reference

[1] S.-H. Kwon, J. Park, et al., Energy Environ. Sci. (2014), 7, 3279 – 3283.

[2] J. Park, S. Song, Y. Yang, S. H. Kwon, E. Sim, Y. S. Kim, J. Am. Chem. Soc. (2017), 139, 10968–10971.

[3] J. Park, Y. Yang, S.-H. Kwon, Y. S. Kim, J. Phys. Chem. Lett. (2015), 6, 745–749

[4] J. Park, Y. Yang, S.-H. Kwon, S. G. Yoon, Y. S. Kim, Nano Energy (2017), 42, 257–261.

[5] Y. Yang, J. Park, S.-H. Kwon, Y. S. Kim, Sci. Rep. (2015), 5, 15695.

[6] J. Park, Y. Yang, S.-H. Kwon, S. G. Yoon, Y. S. Kim, Nano Energy (2017), 42, 257–261.

[7] Y. Yang, J. Park, S. G. Yoon, Y. S. Kim, Nano Energy (2017), 40, 447–453.

[8] S. H. Kwon, W. K. Kim, J. Park, Y. Yang, B. Yoo, C. J. Han and Y. S. Kim, ACS Appl. Mater. Interfaces 8 (2016) 24579-24584.

Chapter 2 Fundamental and Literature Review

2.1 Working mechanism of ionovoltaic device

In the early stage studies of ionovoltaic device, there were various hypotheses about the working mechanism. For example, there were hypotheses about various phenomena that could generate electricity by contact with water, such as streaming current, electrostatic attraction, EDL modulations, and so on [1]. Through the change of the types and concentration of the ion in the water droplet, it was found that the electricity is generated by the modulation of the EDL, that is, the adsorption and desorption of ions, especially cations [Fig. 2.1][1]. Based on these clues, a more advanced ionovoltaic device of Electrolyte-Insulator-Semiconductor(EIS) structure was developed and proved that the dynamics of the ions are the main cause of electricity generation. The schematic image and equivalent circuit of ionovoltaic device with EIS structure are shown [Fig. 2.2]. The characteristic equation of the ionovoltaic device was derived by the DFT simulation and experiments which controlled the dielectric layer thickness, permittivity, and droplet length speed. The derived characteristics equation is as follow (The quantity is summarized in table.1)[2]:

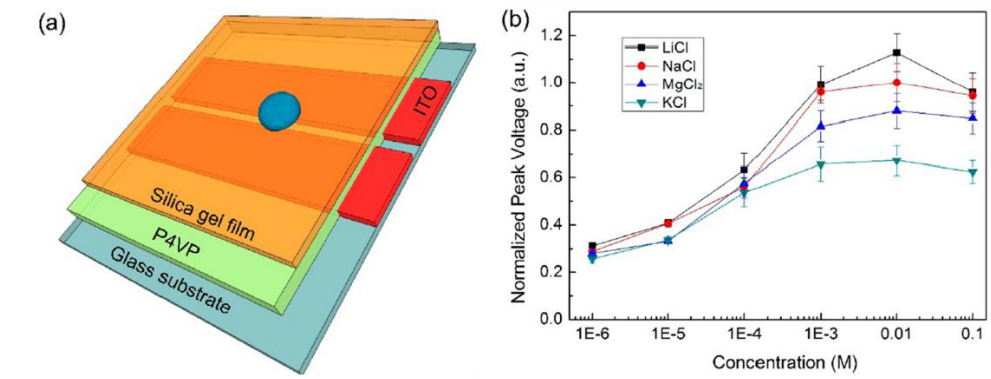

Figure 2. 1 The schematic image of ionovoltaic device and effect of output performance on cations [1].

	QUANTITY
$\boldsymbol{I}$	Output current
$\boldsymbol{V}$	Output voltage
$\boldsymbol{R_{semi}}$	Resistance of semiconductor
$\boldsymbol{v}$	Velocity of droplet
$\boldsymbol{l}$	Length of droplet
$\boldsymbol{R_{\square}}$	Sheet resistance of semiconductor
$\boldsymbol{\varepsilon}$	Permittivity of dielectric layer
$\boldsymbol{d}$	Thickness of dielectric layer
$\sum_i \boldsymbol{\psi_i}$	Potential difference between adsorbed ions and attracted electron

Table 1. The quantity of the characteristics equation [2].

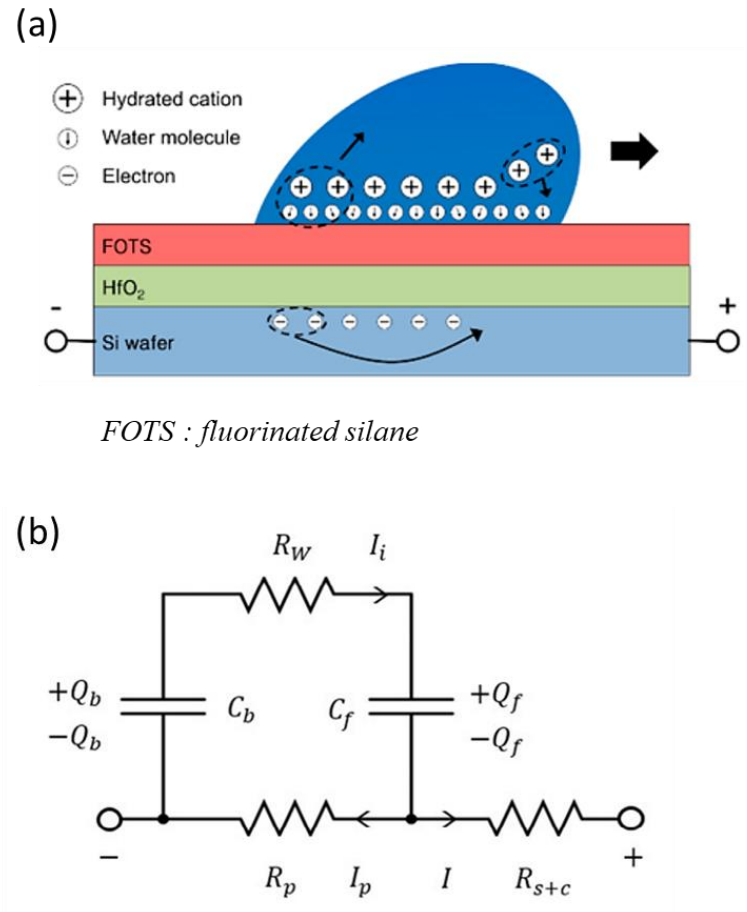

FOTS : fluorinated silane

Figure 2. 2 The schematic image of ionovoltaic device with EIS structure and its equivalent circuit [2].

$$I = -\frac{1}{R_{semi}}(V - vlR_{sq}\frac{\varepsilon}{d}\sum_{i}\psi_i \qquad [Eq.\,2.1]$$

The driving mechanism of the ionovoltaic device identified through Eq 2.1 and experimental data which were previously reported studies is as follows. As the droplet rolls over the hydrophobic layer, there is a new contact area with the solid surface at the front of the droplet, and an area where the contact disappears at the back of the droplet. At this time, the cations are adsorbed by surface potential (mainly negative) electrostatic attraction in the newly formed contact area in front of the droplet. When the cations are adsorbed on the electrode, the density of electrons is instantaneously increased by the Coulomb interactions. On the other hand, at the rear of the water droplet, the adsorbed ions are released by the movement of water droplets and the density of the electrons is lowered. In this process, the current can be measured by the electron density change caused by the adsorption and the desorption of ions occurring at the front and rear side of the droplet through the electrode when the water droplet flows on the ionovoltaic device.

2.2 Components of ionovoltaic device

A typical ionovoltaic device is made up of four elements [Fig. 2.3]; ionic water droplet, hydrophobic layer, insulator and electrodes (with substrates). The water

droplets have ions that play a key role in generating electricity. The movement of the droplet leads to the modulation of the EDL formed at the solid-liquid interface. Recent studies have used water droplets containing monovalent ions such as alkali metals such as Li, Na, K and halide ions such as F, Cl, and Br. Electrodes are mainly used for thin films as the source of electrons. Materials such as graphene, Si wafer, ITO, Cu, Al and so on have been used as electrodes in the ionovoltaic devices [1-6]. The insulating layer serves to prevent the direct transfer of electrons or molecules in the water droplet toward the electrode. A hydrophobic layer facilitates the rolling of water droplets at the interface and prevents the device from getting wet. In addition, the electric double layer (EDL) at the solid-liquid interface, the main source of electricity generation, depends on the nature of the hydrophobic layer. As an ion adsorbent at the solid-liquid interface, the hydrophobic layer is one of the important factors in the ionovoltaic device.

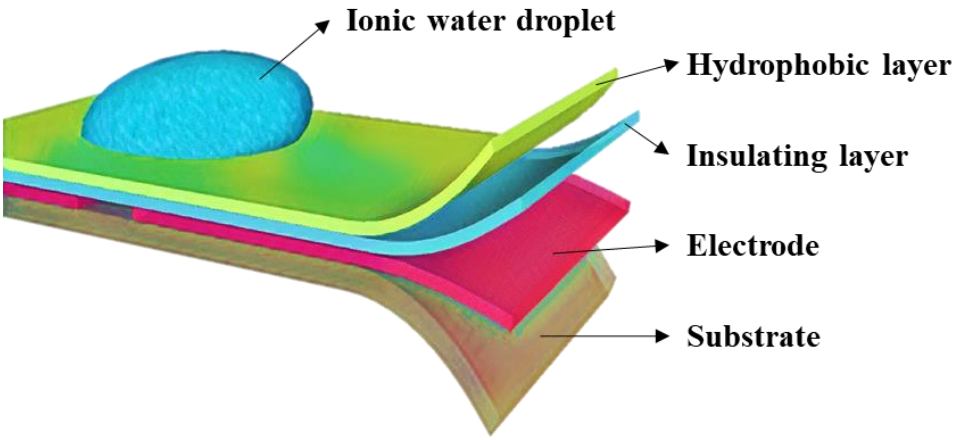

Figure 2. 3 Basic components and structure of ionovoltaic device.

2.2.1. Surface of ionovoltaic devices

The hydrophobic layer in contact with water droplet acts as an adsorbent that protects the device from wetting and adsorbs ions. Thus far, the materials for the hydrophobic layer used in most previous reports were made of a substance which included fluorine atoms with high electro-negativity, such as fluorinated ethylene propylene (FEP) [3,4], polytetrafluoroethylene (PTFE) [5-9] or fluorinated silane [1,2], because these materials exhibit excellent water repellency and offer high electricity generation performance [Fig. 2.4]. Due to the extremely high electro-negativity of fluorine atoms, electrons are drawn from carbon, and strong polarization occurs in the C-F bonding [10]. Therefore, films using fluorinated polymers or fluorinated silane show hydrophobicity with a strong electro-negative function.

The hydrophobic layer used in the ionovoltaic transducer is a representative of two methods of making with fluorinated silanes. We mainly use two methods, chemical vapor deposition method using PFOTS or FOTS, and PFOTS addition to silica gel composed TEOS (tetraethoxysilane). In the case of the chemical vapor deposition method, the substrate to be treated and a small amount of PFOTS or FOTS (about 30 microliters) are placed in a sealed glass vessel and subjected to reaction at 130 ° C for 30 minutes to 2 hours. A vapor deposition

method using a vacuum can be also utilized for the hydrophobic layer. This method forms a self-assembled monolayer, which makes it possible to fabricate a uniform and thin hydrophobic layer for the ionovoltaic device [2]. The silica gel with PFOTS were made by a sol−gel process with the mixed precursor of TEOS and PFOTS in ethanol under acidic conditions. The hydrolysis reactions of PFOTS and TEOS are expressed as following equation, $Si(OC_2H_5)_4 + 4H_2O \rightarrow Si(OH)_4 + 4C_2H_5OH$ and $R_fSi(OC_2H_5)_3 + 3H_2O \rightarrow R_fSi(OH)_3 + 3C_2H_5OH$.($R_f = CF_3(CF_2)_5CH_2CH_2-$. As a hydrophobic layer of the ionovoltaic device, the precursor synthesized for more than 2 hours is coated on the electrode or insulator in thin film form by spin coating and annealing process [1]. In both cases, the ionovoltaic device forms a strong negative surface potential and has a high contact angle of about 100 ° because it has a fluorine functional group [1].

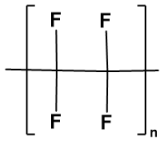

Polytetrafluoroethylene (PTFE)

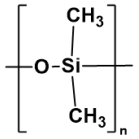

Polydimethylsiloxane (PDMS)

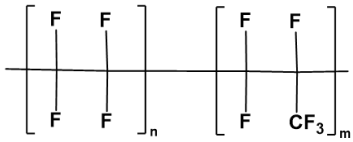

Fluorinated ethylene propylene (FEP)

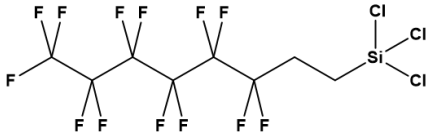

Trichloro(1H,1H,2H,2H-perfluorooctyl)silane (FOTS)

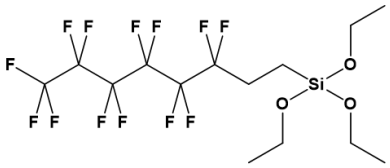

1H,1H,2H,2H-Perfluorooctyltriethoxysilane (PFOTS)

Figure 2. 4 Various materials for the hydrophobic layer of ionovoltaic device.

2.2.2. Structure of Ionovoltaic devices

Electricity is generated in the ionovoltaic device by the change of the electrons density induced by ion adsorption and desorption occurred by the contact between the water droplet and the solid surface. Instantly the area of contact between the water and the solid surface is an important factor, and it produces electricity through asymmetry in the area or through changes in the change of contact line. Therefore, early studies of the device using this water droplet to generate electricity have led to changes in contact area or contact line through the use of two electrodes, either by rolling or vibrating / squeezing of the water droplets [Fig. 2.5]. In these types of devices, the instantaneous contact with the droplet or the change in the contact area causes the generation of the output voltage and current to occur in a peak form. Therefore, in terms of energy storage, it is not efficient due to the low energy density. In addition, there is a disadvantage in views of understanding the ion behavior at the interface, since it must be analyzed through signals for too short a period of time (~0.015s)[1].

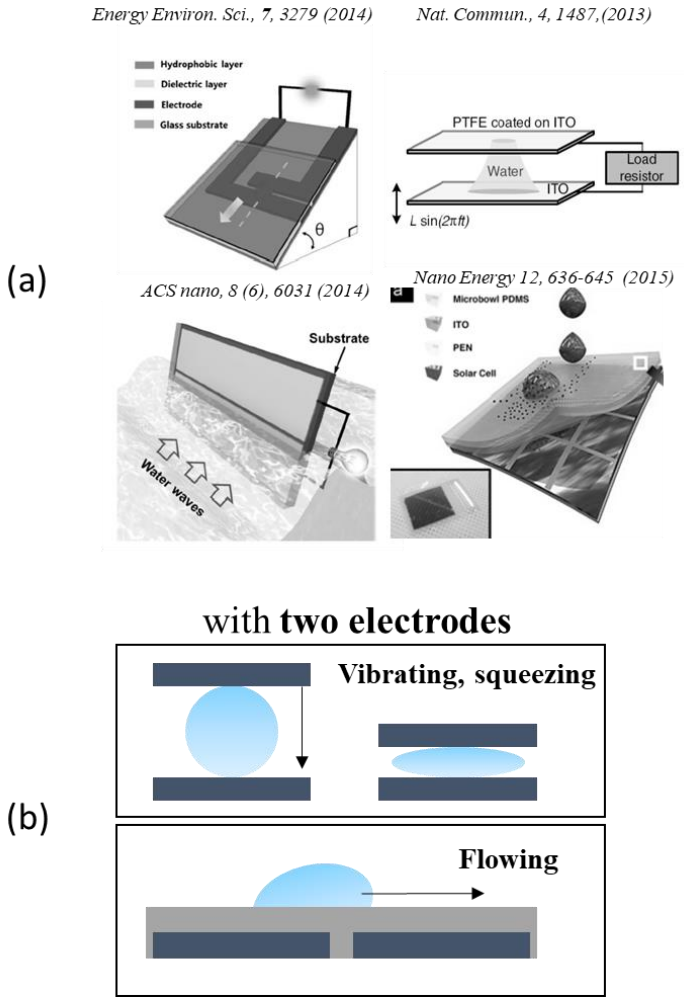

Figure 2. 5 (a) The structure of previous reported devices and (b) schematic image of the basic structure of the ionovoltaic device.

2.4 References

[1] J. Park, Y. Yang, S.-H. Kwon, Y. S. Kim, J. Phys. Chem. Lett. (2015), 6, 745–749

[2] J. Park, S. Song, Y. Yang, S. H. Kwon, E. Sim, Y. S. Kim, J. Am. Chem. Soc. (2017), 139, 10968–10971.

[3] G. Zhu, Y. Su, P. Bai, J. Chen, Q. Jing, W. Yang and Z. L. Wang, ACS Nano 8 (2014) 6031-6037.

[4] L. E. Helseth and X. D. Guo, Langmuir 31 (2015) 3269–3276

[5] Z. H. Lin, G. Cheng, S. Lee, K. C. Pradel and Z. L. Wang, Adv. Mater. 26 (2014) 4690-4696.

[6] S. S. Kwak, S. Lin, J. H. Lee, H. Ryu, T. Y. Kim, H. Zhong, H. Chen and S. W. Kim, ACS Nano 10 (2016) 7297-7302.

[7] S.-B. Jeon, D. Kim, G.-W. Yoon, J.-B. Yoon and Y.-K. Choi, Nano Energy 12 (2015) 636-645.

[8] J. K. Moon, J. Jeong, D. Lee and H. K. Pak, Nat. Commun. 4 (2013) 1487.

[9] Q. Liang, X. Yan, Y. Gu, K. Zhang, M. Liang, S. Lu, X. Zheng and Y. Zhang, Sci. Rep. 5 (2015) 9080.

[10] S. J. Park, K. S. Cho and S. H. Kim, J. Colloid Interface Sci. 272 (2004) 384

Chapter 3 Surface Modification of Ionovoltaic Device and Applications

3.1 Introduction

As explained previous chapters, in the ionovoltaic device, a hydrophobic layer is an important factor because it facilitates the rolling of water droplets at the interface and prevents the device from getting wet. Moreover, the electric double layer (EDL) at the solid-liquid interface, the main source of electricity generation, depends on the nature of the hydrophobic layer. Thus far, the hydrophobic materials used in most previous reports were made of a substance which included fluorine atoms with high electro-negativity. Therefore, films using fluorinated polymers or fluorinated silane show hydrophobicity with a strong electro-negative function. In water motion energy harvesters, different levels of electricity generation performance have been reported depending on the characteristics of the device structures, the electrode materials and the surface roughness levels, but the overall tendencies were similar [1,5,7,12]. When a hydrophobic layer with strong electro-negative functional groups comes into contact with ionic water, the cations in the water are instantaneously adsorbed onto the surface. At this time, electrons flow between the electrodes to neutralize

the adsorbed cations. This phenomenon is verified through the output electricity signal, and the signal is only measured unidirectionally [2,5]. This unidirectional electricity generation is typical in the ionovoltaic device.

In the field of energy harvesting by ion dynamics at a solid-liquid interface, fundamental research on these types of ionic behaviors is essential to understanding the pertinent mechanisms. In addition, an accurate understanding and proper control of ionic behaviors at solid-liquid interfaces are a key to further advances in many applications, including biomedical, energy storage and specific ion sensors. However, thus far few studies have concentrated on fundamentals because most researchers have focused more on improving the performance through structural modifications and material engineering.

Here, for the first time, we introduce an electricity-generating modulation of the water motion active transducer which works through the change of the ionic behavior at the solid-liquid interface through a surface functionality control method. Thus far, there are few studies on electricity modulations through functionality control methods at the solid-liquid interface, as it is difficult to secure hydrophobicity and to control surface functionalities at the same time in a transducer using the motion of water droplets. We successfully secured hydrophobicity in a ionovoltaic device with feasible surface functionality control

at the solid-liquid interface.

3.2 Fabrication of pH-sensitive surface

For pH-sensitive surface of an ionovoltaic device, we used a self-assembled monolayer (SAM) technique [2]. Two types of devices were fabricated; one is an ionovoltaic device treated with PFOTS (1H, 1H, 2H, 2H-perfluorooctyltriethoxy-silane), which is defined here as a SP (silica gel + PFOTS) device, for hydrophobicity with electro-negative function [Fig. 3.1a, 3.2a]. The other one is the ionovoltaic device treated with APTES ((3-aminopropyl) triethoxysilane) and PFOTS, defined here as a SAP (silica gel/APTES/PFOTS) device, for hydrophobicity with electro-positive function [Fig. 3.1b, 3.2b]. In order to fabricate a hydrophobic surface with electro-positive function, two types of molecules with opposite charges were deposited. There are two methods which can be used to make the self-assembled monolayers, using two types of molecules as a single layer: co-adsorption and a stepwise method [18-20]. The co-adsorption technique involves the attachment of two molecules at once with a mixture solution and the stepwise technique refers to a means of attaching second molecules to the voids created when the first molecule creates a partial SAM. Here, we use the stepwise method because it can control more easily and precisely surface functionalities with certain compositions as compared to the co-

adsorption method [20].

For the SP device, a TEOS (tetraethyl orthosilicate) based silica gel film with PFOTS added as an insulator and a hydrophobic layer was spin-coated onto a pre-patterned ITO electrode on glass [1,2,21,22]. In contrast, for the SAP device, an intrinsic TEOS-based silica gel film as an insulator was spin-coated onto a pre-patterned ITO electrode on glass, after which APTES was deposited by dipping in 10 mM of APTES solution for 10 min [23]. For the aqueous deposition of APTES, electrostatic attraction arises with a number of pin-holes, which are induced by the sonication process [8,24]. After sonicating and rinsing the unreacted APTES with distilled water on a void-abundant substrate, the PFOTS was deposited by the CVD (chemical vapor deposition) method in sealed glass vessel for a time of 30 min [25]. The PFOTS reacts with silanol groups on the exposed area of the silica gel film upon a sonication process.

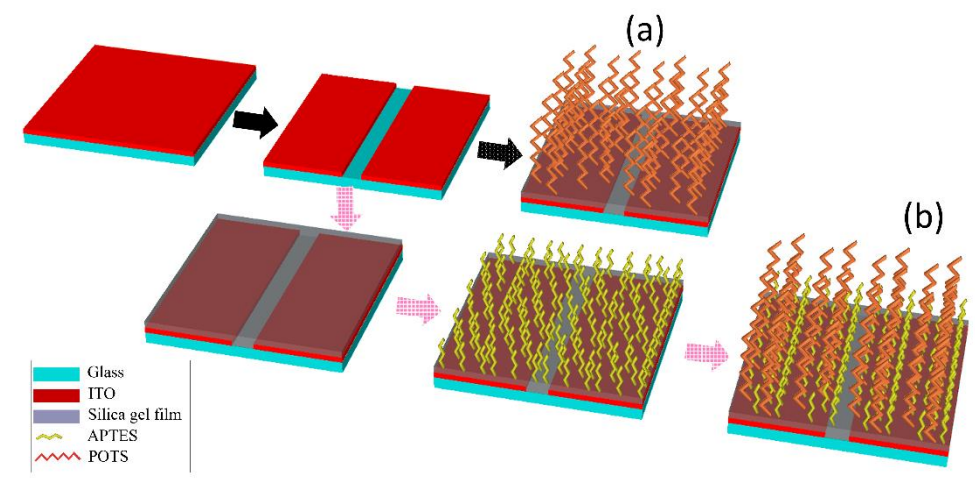

Figure 3. 1 Fabrication processes of the SP(a) and SAP(b) devices.

3.3 Device performances and working mechanism

To evaluate the electrical characteristics of the SP and SAP devices, we measured the electricity generated when water droplets flowed over these transducers. As a representative water droplet, NaCl water droplets (30㎕of 0.01 M) were used. The water droplets were dropped onto the device at a 45-degree angle from a height of 5 mm using a syringe pump [inset image of Fig. 3.2d]. For the SP device, the output voltage and current were measured and found to be 1 V and 0.55 ㎂, respectively [the blue line in Fig. 3.2c, d]. On the other hand, for the SAP active transducer, output voltage in the opposite direction was generated [Fig. 3.2c, d] under identical experimental conditions. The output voltage and current were measured and found to be at -0.4 V and -0.2 ㎂, respectively [the pink line in Fig. 3.2c, d]. For the active transducer coated with only intrinsic silica gel film, although the output voltage and current were low (120 mV and 0.3㎂) compared to the SP device, the output signals were measured in the positive direction. This result verifies that surface functionality control of the active transducer can successfully modulate the behavior of ions and thus demonstrates the possibility of regulating the electrical signals.

The droplets fall on the upper electrode, and a potential difference arises on the front and rear of the droplet as it flows [2,5]. At this time, an electrical signal is

measured at the moment an overlap with the lower electrode part occurs [3]. For the SP device experiment, as in many previous studies [2,5,9], it was confirmed that electricity is generated in one direction (the positive direction in this experiment). This unidirectional electricity generation is caused by the potential difference between the front part, where the cations are instantaneously adsorbed and the rear part, where desorption occurs [Fig. 3.2a]. At this time, electrons move from the electrode to neutralize the adsorbed cations and are measured by the output signal. While the water droplet is rolling in one direction, only adsorption is carried out in the front side, with desorption process performed in the rear side such that the potential difference is maintained. Therefore, the signal is output in only one direction at the moment the droplet overlaps the electrodes below the insulating layer and the hydrophobic layer. Otherwise, in the SAP device, the anion is adsorbed in front of the flowing droplet, and the electricity-generating property is opposite to that of the SP device [Fig. 3.2b]. The main factor of the SAP active transducer having opposite electrical conditions are displayed in the embedded image. NaCl water droplets (30 μL of 0.01 M) were used and were dropped from a height of 5 mm using a syringe pump.

properties is considered as the amine functional groups of the APTES. The amine group existing in the $-NH_2$ form becomes the $-NH_3^+$ form in water, as it is

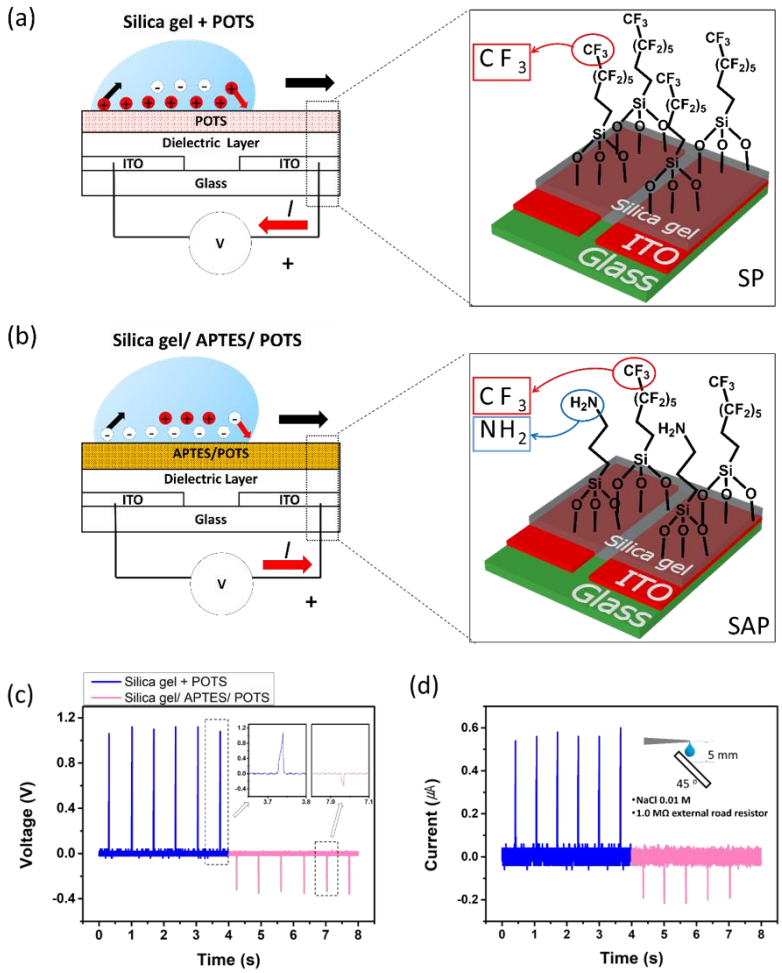

Figure 3. 2 (a, b) Schematic images of SP and SAP devices with functional groups attached and the operating mechanism with a water droplet. (c, d) Electrical performances of the SP (blue line), and SAP (pink line) devices.

protonated by contact with the water droplets and because the SAP device presents a positively charged surface. Amine groups are positively charged as they are protonated, which

is presumed to be the origin of the adsorption of anions initially at the interface as the water droplets pass over the device [5]. Therefore, the generated voltage and the current of the SAP device are measured opposite to that of the SP device identical experimental conditions. As a result, in the SP device, electrons are attracted by the adsorbed cations. Otherwise, in the SAP device, electrons are pushed by the adsorbed anions; thus, the electrical signals of the two active transducers are reversed. As shown in [Fig. 3.2 c, d], the magnitude of the voltage and current in SAP device is one-third level of the output signals in the SP device. This phenomenon is presumed to be due to the fact that the positive charge formed by the amine functional group is reduced by the fluorine functional group with a strong negative charge. This assumption is valid because when the response time of the PFOTS was increased, the output voltage decreased. In addition, the output voltage or current can change depending on the ion types in the water droplet [2]. Therefore, the voltage value at the one-third level in the SAP device is presumed to be due to multiple causes.

We invented an advanced design by changing the surface functionality in the

active transducer, which led to a reversal of the electricity generated under general conditions. Furthermore, this design enables more in-depth research on the ion behavior depending on the surface functionality of the water motion active transducer. According to these results, we verify that the main reason of the reversed signal is the complementary ion motions caused by the surface functionality of the active transducer. Moreover, these results strongly suggest the potential of a good tool with which to observe the ionic behaviors in water at the solid-liquid interface. In water motion active transducers, the generated electricity depends strongly on the ionic characteristics. Specifically, the direction of the electrical signal is induced by the electro-positive or electro-negative function of the surface in active transducers. Therefore, it is essential to prove the presence of functional groups, molecular components and surface energy levels that determine the surface functionalities of active transducers.

To verify the surface characteristics, we used contact angle measurements and an XPS analysis. The contact angle was measured during each fabrication steps of the active transducers [Fig. 3.3a]. The contact angle of the intrinsic silica gel film in the SAP active transducer was measured at 60 degrees. On the other hand, the contact angle of the silica gel film containing PFOTS for the SP device was measured at ~106 degrees. A larger contact angle is exhibited because the fluorine

group of POTS is well exposed to the outside of the silica insulating layer in the SP device. To make hydrophobic layers with electro-positive function using the APTES and PFOTS, the intrinsic silica gel film was treated with ultraviolet ozone (UVO). A completely wet intrinsic silica gel film means that a hydroxyl group is formed on the surface by UVO. The UVO-treated substrate was subsequently immersed in 10 mM of APTES in an aqueous solution for 10 minutes. After the immersion step, the contact angle was measured after a drying process. The contact angle of the APTES-treated substrate was slightly increased, as the APTES was attached to the surface of the intrinsic silica gel film. On the other hand, when PFOTS was deposited onto the APTES-treated substrate, the contact angle was greatly increased to ~108 degrees and sufficient hydrophobicity was secured. The measurement of the contact angle showed that the surface treatment was successful at each step. Moreover, the hydrophobicity necessary for electricity generation was well developed in both the SP and SAP active transducers. Additionally, to identify the surface components that determine the surface functionalities of the active transducers, an XPS analysis was conducted. The peak at ~688 eV corresponds to F1s from the fluorine functional group in the PFOTS [26]. In both types of active transducers, it was confirmed that the fluorine functional groups were well exposed on the surfaces [Fig. 3.3b, c]. Since

the PFOTS and TEOS are used in the SP device, there was no N1s peak near 400 eV, as can be seen from the XPS data in Fig. 3.3d. On the other hand, in the SAP device, N1s peaks were clearly confirmed [Fig. 3.3 f]. The peaks at 399.9 eV and 398.9 eV are evidence that nitrogen exists in the amine group of APTES. The peak located at 399.9 eV between the two deconvoluted peaks means that the nitrogen of APTES exists in the form of a free amine group ($-NH_2$). The peak located at 398.9 eV is ascribed as the signal from the C-N bond of APTES [27]. The result of XPS means that the PFOTS was suitably treated through the F1s peak from the SP device. On the other hand, both the APTES and the PFOTS were feasibly treated through the N1s and the F1s peaks confirmed in the SAP device case. In particular, the XPS results indicate that the electro-positive function formed by the APTES is present only in the case of SAP device.

In order to evaluate the electrical performance capabilities of the active transducers as energy harvesters, the peak voltage and power by an external load resistor were measured [Fig. 3.4a]. As the external resistance increases, the absolute value of the peak voltage increases and the maximum power is generated at 100 KΩ. The maximum power values were measured and found to be ~ 0.6 μW for the SP device and ~0.2 μW for the SAP device. These results show an identical trend in the SP and SAP devices: the absolute value of the peak voltage

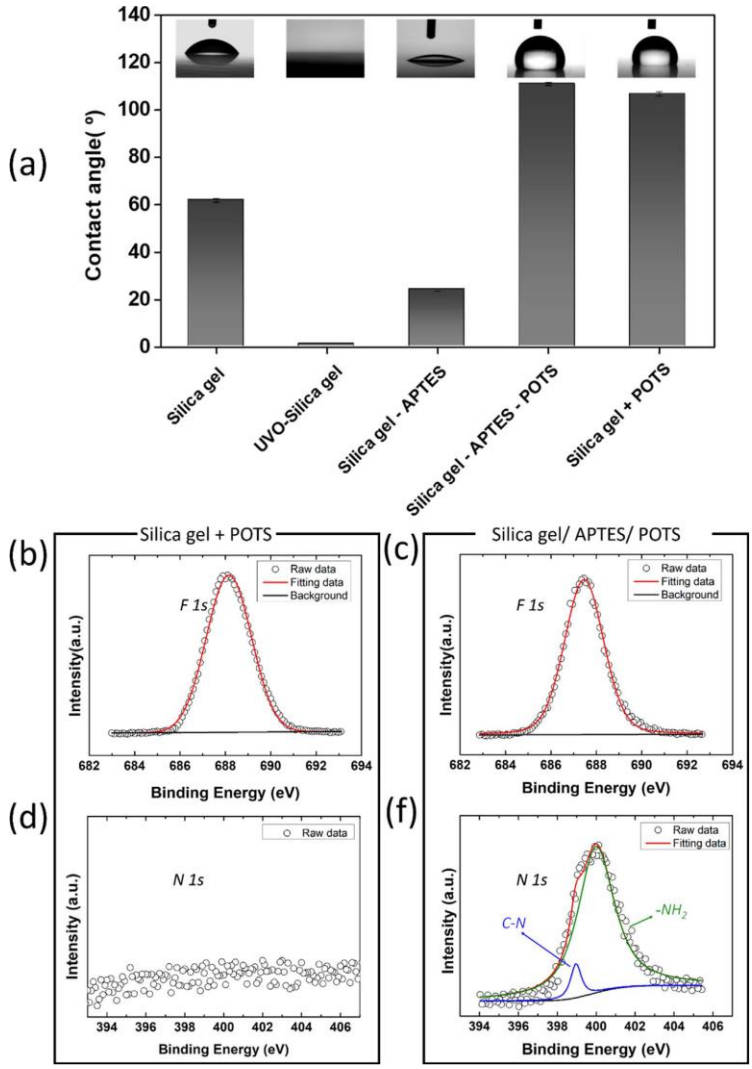

Figure 3. 3(a) Optical images and water contact angle measurements at each stage of the fabrication process. The XPS analysis data of the SP (b, d) and SAP devices (c, f) surfaces. The fluorine spectra and nitrogen spectra were analyzed for the SP and SAP active transducers.

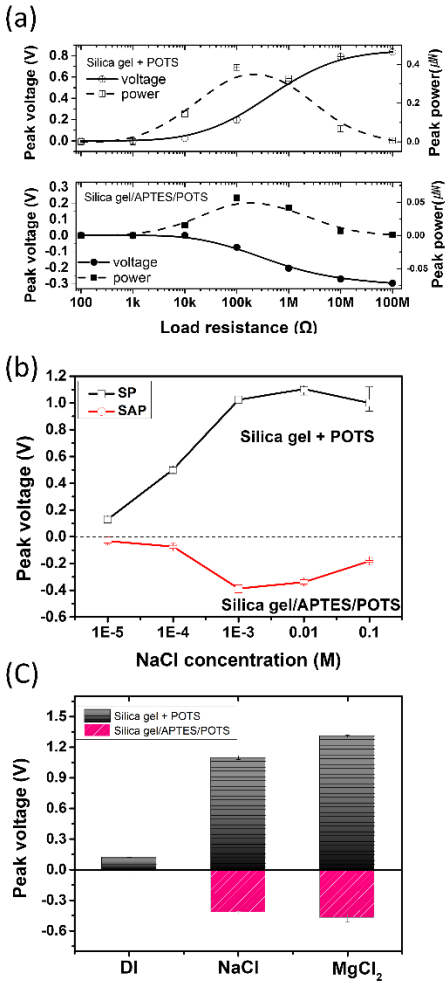

Figure 3. 4(a) The peak voltage measured according to the change in the load resistance for the SP and SAP devices, and power levels obtained by calculations. (b) Measurement of the generated peak voltage by the ion concentration for both devices. (c) Measurement of the generated peak voltage in DI water and in the 10^{-3} M NaCl and MgCl2 solutions. In the experiments, 30 μL water droplets dropped from a height of 5 mm were used.

increases as the external resistance increases. However, due to the surface functionality differences, the directions of the signals generated by the SP and SAP device s are completely reversed.

In both devices, the electrons from the electrode are moved by the adsorbed cations or anions, causing current in the external circuit. In order to verify the influence of the ion concentration, electricity generation according to the NaCl concentration in the range of 10^{-1} to 10^{-5} M was conducted [Fig. 3.4b]. In this case, 30 μL of NaCl water droplets were used and dropped from a height of 5 mm. For the SP active transducer, the magnitude of the generated voltage was influenced by the ion concentration. As the ion concentration was increased, the measured peak voltage value increased and decreased at concentrations of 10^{-2} M or higher. As more ions were adsorbed, more induced electrons appeared. The phenomenon by which the voltage is constant or decreases above a certain concentration appears to be due to the screening effect of counter ions having a charge opposite to that of the initially adsorbed ions [2,5]. For the SAP device, the direction of the voltage was opposite to that in the SP device, and it was found that the voltage decreases at 10^{-2} M or more. The effect of the concentration on the SAP device also shows that the value of the generated absolute voltage increases with more adsorbed ions and then decreases due to the screening effect at or greater than a specific concentration [2,5]. These results also show that the

tendencies are similar but the directions of the signals are reversed in the SP and SAP devices. In addition, it was confirmed that the device respond very sensitively to the ion concentration.

Because the generated signals are affected by ions at the interface between the water and the active transducers, the generated signals strongly depend on the type of ion present. Regarding the ion type tendency, we investigated the generation of electricity with three types of solutions: deionized (DI) water, 10^{-3} M of NaCl, and $MgCl_2$ water solution droplets [Fig. 3.4 c]. In the results of the DI water experiment, a simple noise level appeared in both active transducers. Because there were no ions in the water, electrons cannot be pushed or pulled. In the SP active transducer, the attracting force of the electrons differs according to the type of cation [5]. The output voltages generated with the $MgCl_2$ droplets were higher than the output voltages generated with the NaCl droplets in both the SP and SAP active transducers. In the SAP active transducer, this tendency arose because Mg^{2+} ions can attract more electrons than Na^+ ions at an identical concentration [5]. On the other hand, in the SAP active transducer, a larger value was also using $MgCl_2$ droplets, as the number of Cl^- ions at an identical concentration is twice that with the NaCl droplets. Hence, higher voltage in negative direction is measured while more electrons are pushed during the adsorption process. In this result, it was verified that the electrical

characteristics can be changed depending on both the ion species and the number of ions.

3.4 Application of ionovoltaic device as a pH sensor

The ionovoltaic device with electro-positive surface has pH dependency because of net surface potential variation by the protonation and deprotonation of amine functional groups on the device [Fig. 3.5]. Therefore, considering that the amine functional groups of APTES have their own properties, the high degree of sensitivity to the pH, we developed a SAP device as a self-powered pH sensor toward the realization of practical applications.

3.4.1 pH sensing device performance and working principle

In order to assess the pH sensitivity of the SAP device, the output voltage was measured by dropping acid/base water droplets ranging from pH 2 to 12. The acid and base solutions were titrated into DI water using HCl and NaOH. The output signals were measured in the negative direction in the acid region, and the positive signals were measured in the base region [Fig. 3.6a]. In the acid region, the amine functional groups of the SAP active transducer are mostly protonated and are

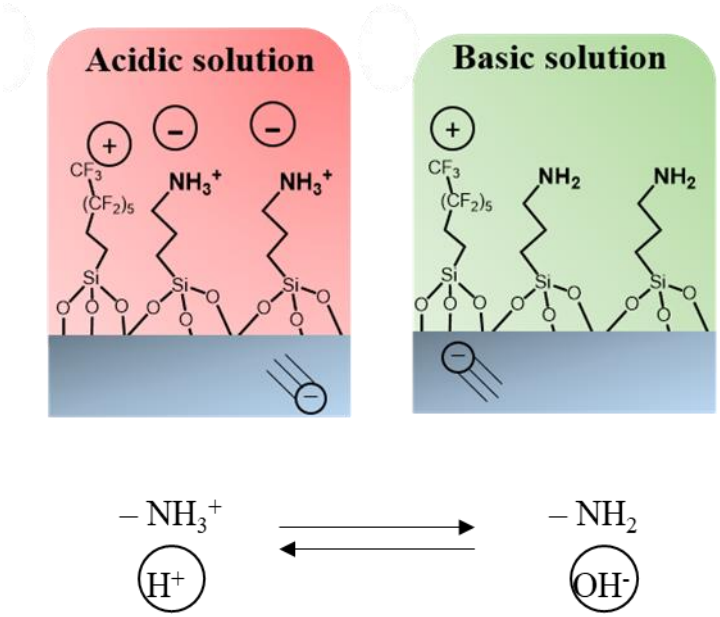

Figure 3. 5 Net surface potential variation of ionovoltaic device by the pH of solutions and ion dynamic at the solid-liquid interface.

present in the NH_3^+ form. As a result, the electro-positive function of the SAP active transducer become strong. Therefore, the anions are attracted more and the absolute value of the generated voltage increases. On the other hand, in the base region, the amine functional groups are present in the NH_2 form due to deprotonation. As a result, the cation comes first due to the fluorine functional group. Therefore, the voltage is measured in a direction identical to that noted with the SP device. In the range of pH 6 to 9, the SAP had a small voltage value, close to a noise level, because the number of ions present in the range of pH 6 to 9 is considerably lower than in other pH ranges.

In order to confirm the reliability of the SAP device as a pH sensor, repeated experiments were carried out involving the dropping of acid and base water droplets [Fig. 3.6b]. Water droplets at pH 3, 7, 11 and 7 were repeatedly dropped at a height of 5 mm. The generated voltage of 0.34 V was repeatedly measured under basic conditions, and voltage of approximately - 0.35 V was repeatedly measured under acidic conditions. The plotted voltages are the calculated average voltages measured when 12 droplets were dropped on the SAP active transducer at pH 3, 7, and 11 in each case. These results show that the signals were consistently generated in the acid and base regions and that reliability was secured as a self-powered pH sensor. One important aspect here is the direction of the

noise level signals from the water droplets at pH 7. The noise-level signals were measured with the pH 7 droplets dropped between acid and base droplets because there were too few ions to pull or push the electrons in the electrode. However, the noise-level signals were measured in the negative direction after the contact by the pH 3 droplet and in the positive direction after the contact of the pH 11 droplet. This result implies that the

changed functionality of the surface due to the droplets which made first contact (pH 3 or 11) affects the generation of electricity by the contact of the second droplet (pH 7). In order to identify the influence of the surface functionality due to the water droplet which initially makes contact, after dropping the pH 11 droplets, the voltage of the SAP device was measured by dropping pH 3 droplets (skipping the pH 7 droplets). As a result, we found through real-time measurements that the properties of the surface functionality changed during the experiment involving the dropping of water droplets when changing the pH from 11 to 3 [Fig. 3.6c]. When dropping the pH 3 droplets immediately after dropping the pH 11 droplets, a three-step process was observed in the generated signals, and it means that the surface functionality changed. The steps were as follows. (**1)** The voltage value generated in the positive direction gradually decreased**. (2)** Signals are generated simultaneously in the positive and the negative directions.

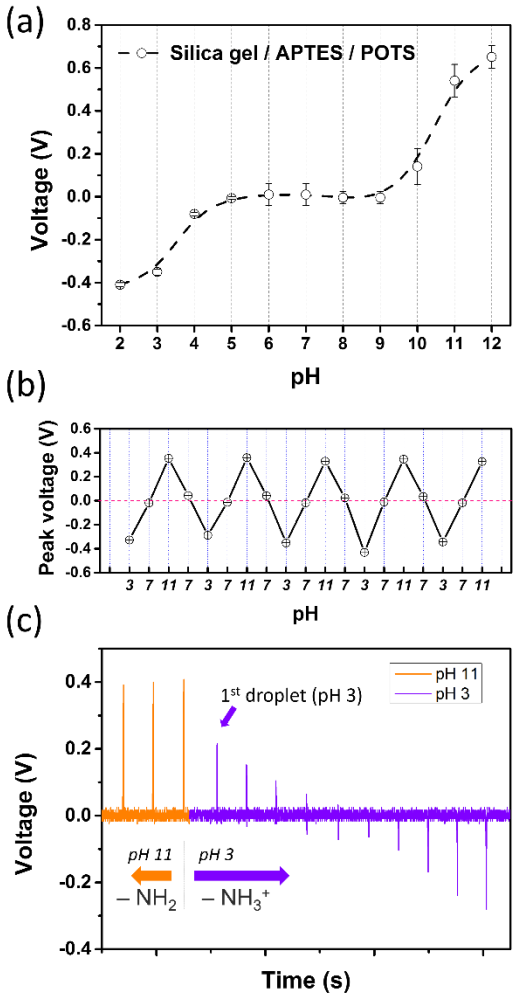

Figure 3. 6 (a) Peak voltage measurement according to various pH levels for the SAP device. (b) Reproduction and reliability evaluation by alternately dropping acid (pH 3) and base (pH 11) droplets. Droplets at pH 7 were dropped between the dropping of acid and base water droplets. (c) Voltage measurement upon the dropping of acid water droplets immediately after the dropping of base water droplets.

(3) The signal is output in a completely negative direction. When the pH 11 droplets were dropped onto the SAP device, the output signals were generated in a positive direction. Subsequently, when the pH 3 droplets were immediately dropped, the electrical signal was not directly reversed at that instance. After the dropping of a few pH 3 droplets, the signal was stabilized and reverse voltage was generated in the negative direction. This real-time change of the output voltage stems from the gradual protonation of the deprotonated amine group by the H_3O^+ in the acid droplets. During the protonation of the amine group in APTES, the surface functionality of the device is changed from electro-negative to electro-positive; thus, the overall electrical properties change. During the process of changing the surface functionality, when the two characteristics of electro-negative and electro-positive functions overlap, the AC signal appears for a while.

In these results, the amine functional groups in the SAP device reacted to the various pH levels, converting the functionality of the device surface and showing different output signals in the acid and base conditions. This achievement demonstrates the potential to realize a self-powered pH sensor that differs from various conventional pH sensing devices such as an ISFET (ion-sensitive field-effect transistor) [28-30]. It should be noted that pH sensors using ISFETs require

complex fabrication processes and external power sources. In contrast, the SAP device as a pH sensor in this study has the advantage of a simple fabrication process and self-powered device. We believe that it can serve as a new type of self-powered pH sensor. In addition, it is expected that measuring the change in the surface functionality in real time can be utilized not only for pH sensing but also for the detection of various aqueous solution substances, such as ions and biomolecules.

3.5 Application of ionovoltaic device as a urea detector

Detection and concentration measurement of urea are widely used for human health check. Urea in body fluids, for example in urine and blood, is an important indicator when diagnosing human organs such as the kidney and liver [35-37]. Despite the considerable body of research in this area, limitations such as the need for an external power source and the complex operation of electrochemical flow cells remain.

Herein, we introduce a novel urea sensing method that accomplishes urea detection with a single droplet of an analyte using a pH-sensitive ionovoltaic transducer and an enzyme attached glass probe. An ionovoltaic transducer converts ion dynamic phenomena at the solid-liquid interface directly into

electrical signals without an external power source or additional electrochemical flow cells[52,53]. With a single droplet of an analyte containing urea (140$\mu\ell$), the output voltage is inverted within two minutes by surface potential changes induced by the urea decomposition depending on urea concentration in the range of 1 to 50 mM. Furthermore, in a selective experiment with various biomolecules such as glucose, ascorbic acid, and lactic acid, the inversion of the output voltage occurred selectively only in the urea containing analyte, which confirmed the feasibility of the proposed unique biosensor. We believe that the combination of the ionovoltaic transducer and the enzyme attached probe will greatly broaden the scope of applications of this novel biosensor.

3.5.1 Fabrication method

The ionovoltaic urea sensor consists of three parts: a probe with urease, an ionovoltaic transducer with a pH-sensitive surface, and an analyte droplet, as shown in the schematic image in [Fig. 3.7a]. With regard to the probe, three layers of polyethylenimine (PEI) and urease were deposited onto a 1x1 cm^2 region of a glass plate by a layer-by-layer (LBL) method which uses electrostatic attraction [Fig. 3.7a, enlarged image]. Given that the aqueous analyte solution penetrates into the PEI-urease layer, the decomposition performance of the urea is improved

as the number of enzyme layers is increased [47]. In order to verify the attachment of the enzyme at the tip of the probe, topographic images of the urease and PEI to the attached surface were confirmed using AFM. As shown in Fig. 3.7b, the urease is immobilized tightly by electrostatic attraction at a very high density. Despite measurements after a sufficient rinse procedure, the AFM image shows that the enzyme is firmly attached to the glass plate. For the ionovoltaic transducer, two ITO (indium tin oxide) films deposited (120 nm) onto a glass substrate with a 2 mm gap were used as electrodes. On the electrodes, unlinked PDMS was coated as an insulating layer with a thickness of 10 micrometers using a spin coater. After a cross-linking process on a hot plate, both APTES and PFOTS were deposited via a stepwise method to make an ionovoltaic transducer with a pH-sensitive surface. For the urea solution, two types were prepared: 0.1 mM of NaCl and a pH 5 solution titrated with HCl. We defined the experiment using a urea analyte droplet with 0.1 mM of the NaCl solution as a normal mode and with a pH 5 solution as an expanded mode. The distance between the probe and the transducer was kept at 3 mm and the measurements were conducted with 140 microliters of the urea solution. The output voltage and surface zeta potential were measured with an oscilloscope (DPO-2024) and a SurPASS™ 3 (Anton Paar), respectively.

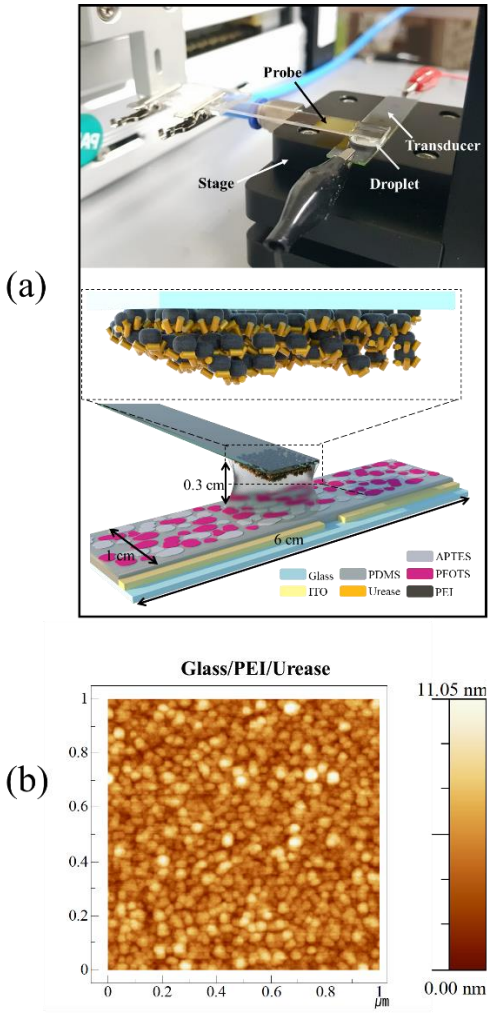

Figure 3. 7 Fabrication method of the ionovoltaic urea biosensor and an AFM image of the probe with urease. (a) The length and width of the transducer are 6 and 1 cm, respectively. The gap between the probe and the transducer is 0.3 cm. Three layers of urease-PEI were deposited onto a glass probe by the LBL method (enlarged image). (b) AFM image of the urease on the probe.

3.5.2 Device performance and working mechanism

The ionovoltaic urea sensor utilizes a method of measuring the output voltages according to the change in the pH of the urea droplet as the urea is decomposed by the urease on the probe. Therefore, the relationship between the output voltages and the surface zeta potentials according to the pH variation of the droplets on the ionovoltaic transducer was investigated. As shown in Fig. 3.8a, the water droplet is dragged by the probe so that it is put into reciprocating motion at a speed of 6 cm/s. Throughout the droplet movement, the electrons in the electrodes are repulsed and attracted by the adsorption and desorption of the ions at the solid-liquid interface. In the ionovoltaic transducer, because both amine groups with a positive charge and fluorine groups with a negative charge are present on the same surface, the net surface potential is determined by the protonation/deprotonation of the amine groups by the hydrogen/hydroxyl ions in the solution when it is in contact. In an acidic solution (Fig. 3.8b and 3.9a), the net surface potential is positive as the amine on the surface of the ionovoltaic transducer is protonated by the hydrogen ions [Fig. 3.9a]. As a result, the anions (e.g., Cl^-) in the front of droplet are adsorbed at the liquid-solid interface and the electrons in the electrode are repulsed out. On the other hand, in a basic solution [Fig. 3.8c and 3.9b], the amine group is deprotonated by the hydroxyl ions and

the net surface potential becomes negative. Therefore, the cations (e.g., Na^+) are adsorbed the front of droplet and attract electrons in the electrodes [18, 22]. The net surface potential changes in the ionovoltaic transducer according to the pH of the water droplets and the output voltage changes according to the surface potential. Therefore, the surface zeta potential and the output voltages according to the pH in the ionovoltaic transducer are investigated [Fig. 2.9c]. In the acidic region (below pH 7), the number of protonated amines increases and the surface zeta potential increases in the positive direction. As a result, the output voltage is increased in the negative direction as the electrons are repulsed out by the adsorption of more anions on the surface. In the pH range of 7 to 9, the charges of the amine and the fluorine groups on the surface were balanced and the surface zeta potential became zero. As the surface zeta potential approaches zero, the output voltage of the device is also close to zero. From pH 10 and onwards, the surface potential is reversed to negative by the deprotonation of the amine group. As a result, the electrons are attracted by the adsorption of more cations on the surface and the voltage increases in the positive direction. The reversal of the output voltage is related to the inversion of the surface potential. We previously derived the characteristic equation of an ionovoltaic device which had a high-resistivity semiconductor as a mono-electrode [51]. Because this urea sensor had

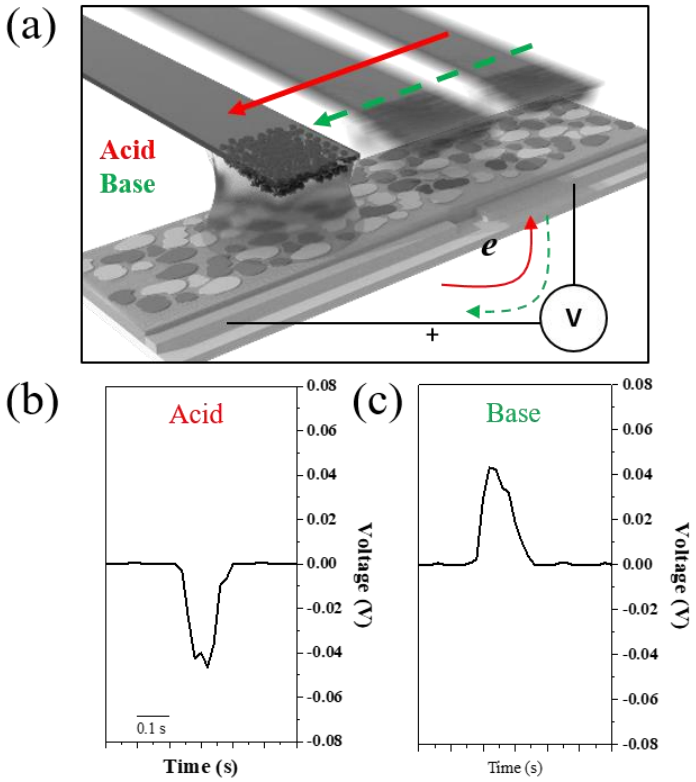

Figure 3. 8 Schematic images of the operating mechanism and measured surface zeta potential in acid and base conditions. (a) Operating condition and direction of the output current in an acid and a base. (b) Output voltage and schematic image of the surface in the acidic condition. (c) Output voltage and schematic image of the surface in the basic condition.

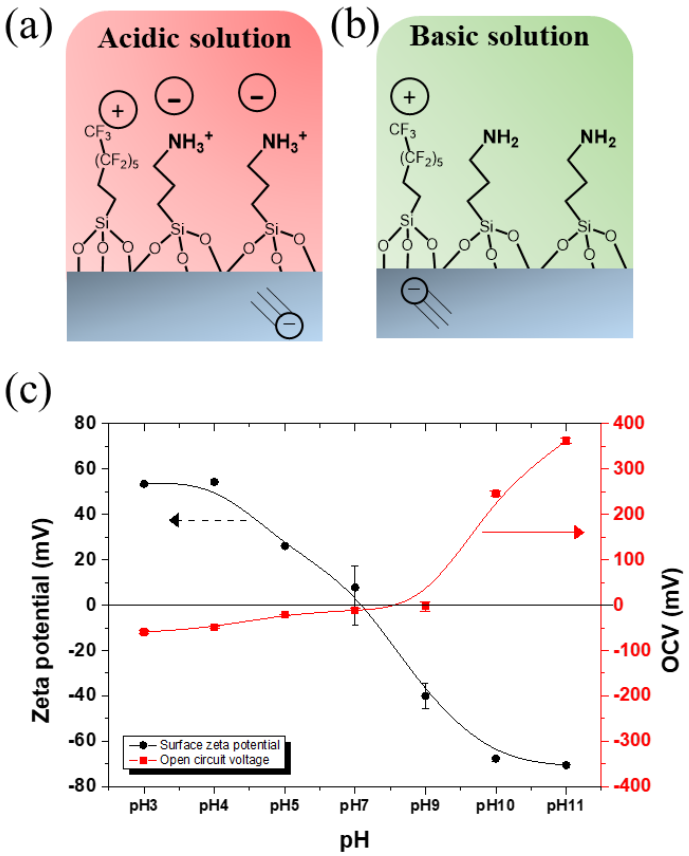

Figure 3. 9 Schematic images of the interface and measured surface zeta potential in acid and base conditions. (a) Schematic images of the surfaces in the acidic condition and (b) in the basic condition. (c) Measured OCV and surface zeta potential of the ionovoltaic transducer according to variations of the pH.

two parallel conductors (ITO) as an electrode, the parallel resistance component is infinite and the series resistance is zero compared to earlier ionovoltaic devices. The characteristic equation of the ionovoltaic urea sensor can be derived by changing the resistance component, as follows.

$$I = -\frac{1}{R_w}\left(V - vWR_w\frac{\varepsilon}{d}\sum_i \psi_i\right) \qquad [eq.\,3.1]$$

Here, I and V are respectively the output current and voltage of the transducer, R_w is the resistance of the water droplet, v and W are the speed and width of the water droplet. ε and d are respectively the permittivity and thickness of the dielectric layer. $\sum_i \psi_i$ represents the potential difference between the adsorbed ions and attracted electrons. This potential difference is also expressed as the difference between the zeta potential (ζ), which is the potential drop across the diffuse layer, and the interfacial potential (ψ_{ds}) at the electrode-dielectric layer interface. Hence, $\sum_i \boldsymbol{\psi_i} = \boldsymbol{\psi_{ds}} - \boldsymbol{\zeta}$.

Therefore, the open-circuit voltage is expressed by the following equation:

$$\boldsymbol{V_{oc}} = \boldsymbol{vWR_w\frac{\varepsilon}{d}(\psi_{ds} - \zeta)} \qquad [eq.\,3.2]$$

As indicated by Eq. (3.2), V_{oc} is determined by the velocity of the droplet, the permittivity, and by the other factors, but the sign is determined according to the sign of the surface zeta potential [Fig. 2.9c]. The immobilized urease on the probe catalyzes the hydrolysis of urea, which produces NH_4^+, HCO_2^- and OH^- (Eq. (3.3))

[36, 47].

$$(NH_2)_2CO + 3H_2O \xrightarrow{urease} 2NH_4^+ + OH^- + HCO_3^- \qquad [eq.\,3.3]$$

Over time, the hydroxyl ions produced by the decomposition of urea diffuse into the droplet and change the pH of the droplet. Diffused hydroxyl ions deprotonate the amine on the ionovoltaic surface and change the net surface potential. As a result, if urea is present in the analyte, the surface zeta potential changes as the decomposition process continues, and the sign of V_{oc} can be reversed [Fig. 3.10a]. The time at which the output voltage becomes zero is defined as the voltage-inversion time (VIT). Because the movement of the probe is a reciprocating motion, the electric signals are measured in the forward and backward motions (Fig. 3.10a, red and blue lines). The output voltages for about 100 seconds can be divided into four sections according to the decomposition of urea, the pH variation of the droplet, and the change in the surface potential [Fig. 3.10b, I-IV].

In region I, the enzyme catalyzes the hydrolysis of the urea and the composition of the droplet begins to change. However, the variation of the output voltage during the initial about ten seconds is negligible because OH^- does not directly react with the surface of the ionovoltaic transducer. In region II, the diffused hydroxyl ions attack the surface of the ionovoltaic transducer and start to deprotonate the amine group. As the amine group deprotonates, the net surface

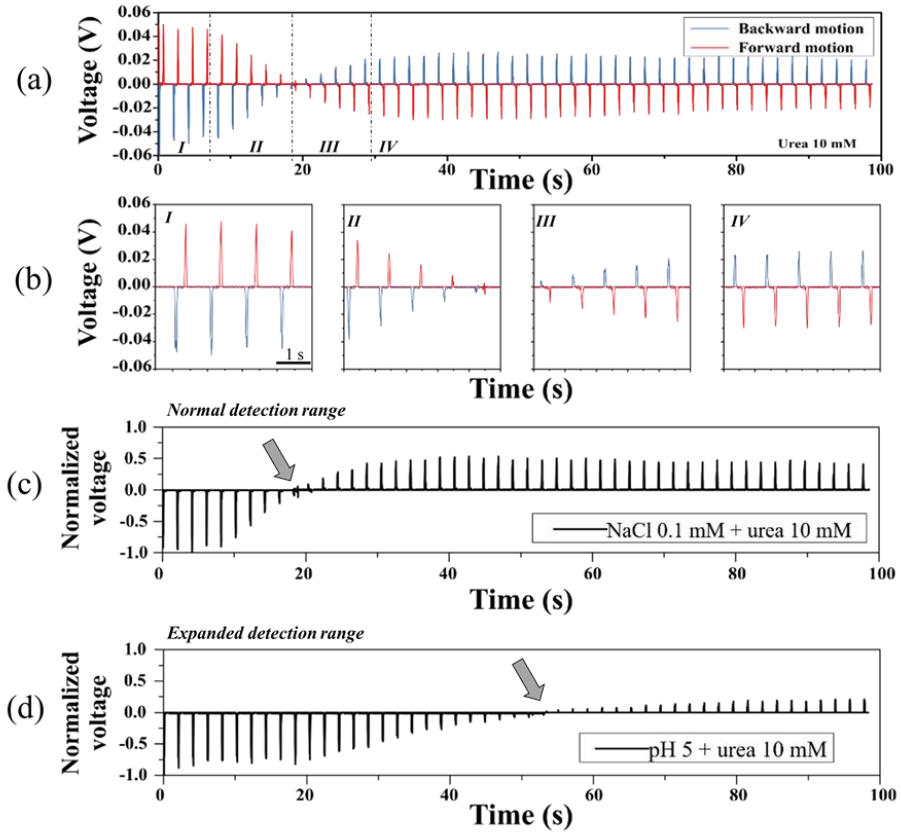

Figure 3. 10 Performance of the ionovoltaic urea sensor. (a) The measured output voltage with 10 mM of urea in the normal mode with the speed of the probe set to 6 cm/s. The output voltage was measured in all cases during backward/forward motions, and it can be divided into four regions. (b) Enlarged data of the output voltage measured in the four sections. (c, d) Output voltages in the normal mode and expanded mode. In the data, only the output voltage during backward motion was extracted and normalized.

potential changes from positive to zero, approaching the isoelectric point. In this case, the voltage generated by the anions in the transducer rapidly decreases to zero. As the urea continues to decompose

(region III), the remaining amines are deprotonated and the net surface potential changes from 0 to negative, adsorbing more cations at the solid-liquid interface. As a result, the output voltage is measured in the positive direction. After most of the amine functional groups become deprotonated by the decomposed urea, the output voltage saturates, as shown in region IV. This explanation is reliable based on the results in the expanded mode using a urea analyte droplet with the pH 5 solution.

The output voltages in the normal mode and expanded mode (extracted and normalized the output voltages during backward motion) are shown in Fig. 3.10c, 3.10d respectively. In the expanded mode, the duration of region I is longer than that in the normal mode. This result indicates that the hydroxyl ion from the decomposition of urea requires more time to react with the amine functional group on the surface of the transducer. The hydroxyl ions cannot reach the surface due to the recombination with the hydrogen ions in the solution of the expanded mode (pH 5). In other words, the inversion of the surface potential, which causes the voltage to reverse, is changed slowly by the recombination reaction. As indicated by this result, the amount of diffused ions can be controlled by the initial test solution,

suggesting the possibility of tuning the detection range of the urea concentration.

The detection range of the ionovoltaic sensor is verified through the VITs when it is between 1 and 10 mM in the normal mode. Above a concentration of 1 mM, all of the measured output voltages were inverted and the VITs were 18, 42, and 120 seconds at 10, 5, and 1 mM, respectively [Fig. 3.11, 3.12a]. The measured output voltage at 0.5 mM for about 100 seconds showed a decrease in the signal but the voltage did not drop to zero [Fig. 3.11e]. This result means that the amine groups present on the transducer surface are not completely deprotonated at a concentration of 0.5 mM. That is, below 0.5 mM, the net surface potential of the transducer is still positive. On the other hand, with more than 10 mM of urea (50 mM), the VITs were nearly identical at about 18 s, and it can be deduced that the amine groups on the ionovoltaic transducer are fully deprotonated well above 10 mM. At a concentration of 10 mM or more, it is possible to discriminate the inversion time difference even at a concentration of 10 mM or more through measurements in the expanded mode using the acidic solution as an initial solution. In the case of 10 mM in the expanded mode, the hydroxyl ions formed by urea decomposition are recombined with the hydrogen ions present in the acid water. Because the hydroxyl ions capable of deprotonating the amine groups on the surface are lost during the recombination process, the inversion time becomes longer. On the other hand, at 50 mM of urea in

the expanded mode, the output voltage is reversed even more rapidly after the recombination because there are enough hydroxyl ions to protonate the amine group on the surface. Therefore, as shown in [Fig. 3.13b], the difference in the VIT between the 10 mM and 50 mM cases in the extended mode is 16.7 seconds, which can be distinguished sufficiently through the VIT at both concentrations. As shown in these results, the urea determination and concentration analogy via the VIT is very intuitive and easy to understand. Also, the detection range can be controlled through the pH adjustment of the urea solution.

As shown by the above results, the VIT can be controlled by the initial pH of the urea solution, but it can also be controlled by the amount of enzyme attached to the probe. Because the LBL method can increase or decrease the number of enzymes sequentially, the total amount of enzyme varies depending on the number of layers, and the hydrolysis of urea can be controlled. When the number of layers of urease-PEI is increased stepwise from one to three layers, as the total urease is increased, more urea decomposition occurs at once and the VIT can be reduced at the same concentration of urea [Fig. 13a] This result shows that the decomposition of urea

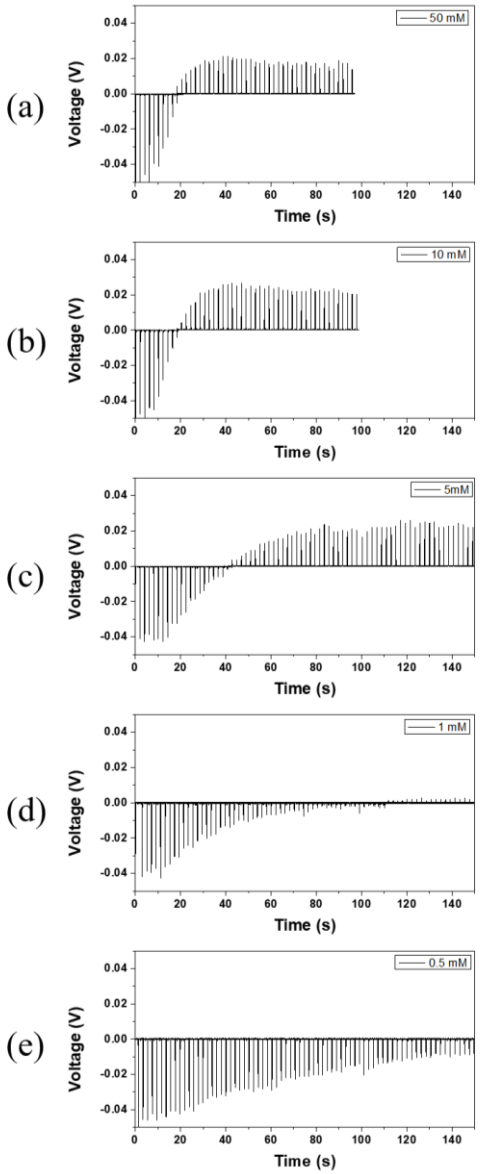

Figure 3. 11 Measured output voltage (backward motion only) according to the urea concentration in the normal mode: (a) 50 mM, (b) 10 mM, (c) 5 mM, (d) 1 mM and (e) 0.5 mM.

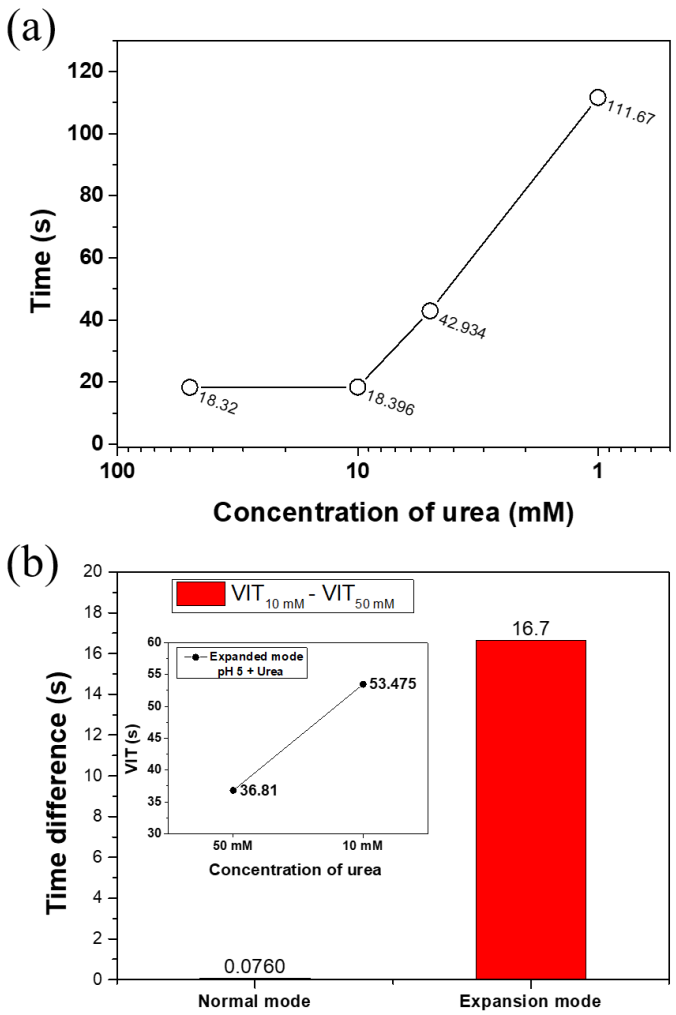

Figure 3. 12 Measured inversion time according to the urea concentration. (a) VIT according to the urea concentration in the normal mode within the range of 50 mM to 1 mM. (b) VIT comparison in the normal and expanded modes with 10 and 50 mM of urea.

and the inversion time vary linearly with the entire amount of urea on the probe, meaning that the probing time can be easily controlled through the LBL method.

From a commercial standpoint, the reusability of the sensor is an important factor to reduce the detection cost. In addition, the activity of the enzyme can be confirmed by verifying the reusability of the sensor. To verify the reusability and reliability of the ionovoltaic urea sensor, the effects of the reuse on the output voltage were studied. Reusability assessments of the probe and transducer were conducted with 10 mM of urea in the normal mode. The probe and the transducer were rinsed with DI water after the measurement, dried using N_2 gas, after which another measurement was taken. As a result of the reusability test [Fig. 13b], the VIT in the first test was 18.3 seconds, with the VIT then maintained between 20 and 22 seconds for ensuing tests. The measured times were traced to the concentration, and the difference in the concentrations of urea between 18.3 seconds and 22 seconds was found to be close to 0.8 mM, which confirmed the possibility of reusing the sensor successfully.

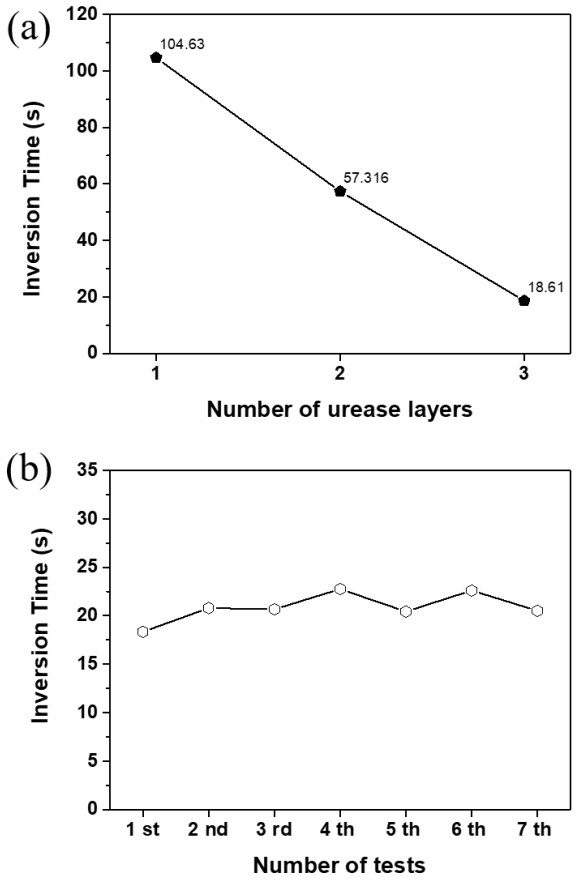

Figure 3. 13 Measured VIT according to the number of urease layers and reusability test results. (a) VIT measured by attaching urease-PEI layers from one layer to three layers to the probe. The VITs were measured in the normal mode with 10mM of urea. (b) A reusability test was carried out using three layers of urease-PEI with 10 mM of urea. The transducer and probe were washed with DI water and dried with N_2 gas after each test.

3.5.3 Possibility of ionovoltaic urea detector as a biosensor

Regarding the effectiveness of ionovoltaic transducer as a biosensor, its selectivity for urea was investigated. In the selectivity experiment, the output voltages were measured in the ionovoltaic urea sensor with analyte solutions containing 10 mM of urea, ascorbic acid (AA), NaCl, lactic acid (LA), and glucose (Glu) with the urease attached probe [Fig. 14a to 14e]. In addition, the VIT was measured without urease on the probe to study the effects of urea decomposition by urease. As shown in Fig. 14b to 14e, voltage inversion did not occur in the AA, LA, Glu, or NaCl cases. Voltage inversion also did not occur in the urea case when sensing with a urease free probe [Fig. 14f]. These results indicate that the ionovoltaic urea sensor works due to the urea-urease reaction and the sensor can determine the presence of urea intuitively through voltage inversion. In addition, the ionovoltaic urea sensor was not affected by other biological molecules in body fluids such as glucose or lactic acid. The results of the reusability and selectivity for urea strongly suggest the possibility of the proposed sensor finding use as a biosensor.

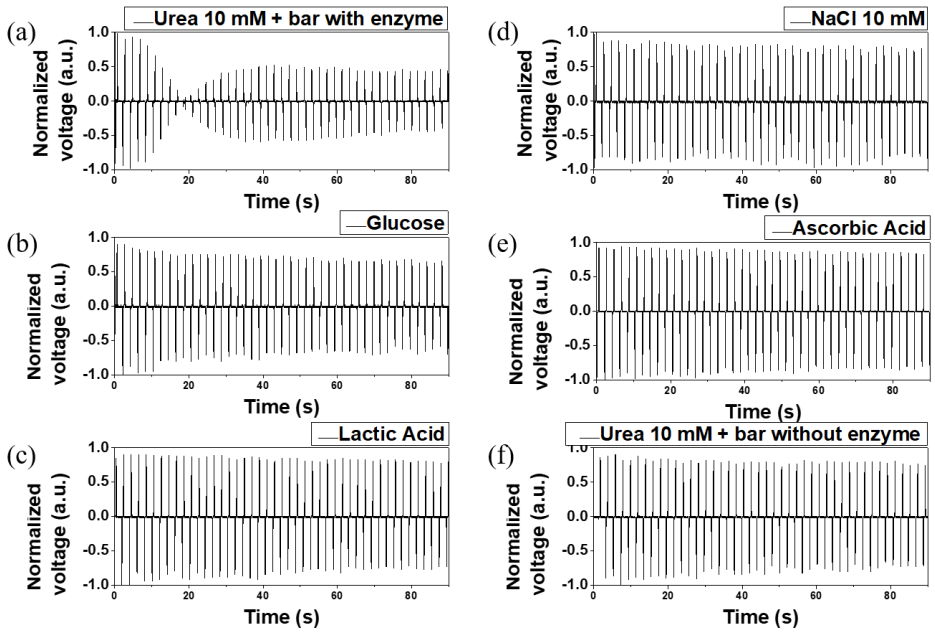

Figure 3. 14 Effects of voltage inversion for the ionovoltaic urea sensor with (a) the presence/(f) absence of urease on the glass probe with 10 mM of urea. Confirmation of selectivity against 10 mM of (b) glucose, (c) lactic acid, (d) NaCl and (e) ascorbic acid by the ionovoltaic urea sensor with the urease probe.

3.6 Conclusion

In summary, we successfully modulated electrical signals by changing the ionic behavior through surface modification of the ionovoltaic devices. In addition, we demonstrated the practical usability of ionovoltaic device as a novel self-powered pH sensor and urea detector using the characteristics of the sensitive reactions with ions.

In this work, we implemented an effective experimental design to control the surface functionality to derive the effects of an electrical signal reversal with common solutions, in this case NaCl water. Moreover, the fundamental study carried out with this experimental design made it possible to gain a deeper understanding of what happens at the solid-liquid interface of the water motion active transducers. In practically, we believe that our research offers good potential for those studying novel ion detectors owing to the controllability of surface functionalities and the high sensitivity of ion characteristics for the generation of electricity by the device.

Furthermore, we also successfully demonstrated a new type of urea sensor that is simple and intuitive using a urease attached probe with an ionovoltaic transducer with modified hydrophobic surface and verified the urea detection

principle. The urea was determined by reversing the output voltage, and the concentration was traced by measuring the voltage inversion time. In an analyte droplet of 140 microliters, the detection range is from 1 to 50 mM (normal and expanded modes) and the detection times are between 18 and 110 seconds. This ionovoltaic urea sensor was validated for urea selectivity, reproducibility, and reliability. The ionovoltaic urea sensor does not require a cumbersome injection system such as a micro-chemical flow cell and can therefore easily undertake measurements with a single droplet. Moreover, the wasting of analytical solutions can be reduced. Unlike other sensors such as those that rely on a FET [47-50] to supply external bias to the source or gate, the ionovoltaic transducer itself is a self-powered device and is therefore well suited for analyzing aqueous based biological liquids. When analyzing the measured signals, one advantage is that the presence of urea can be determined intuitively through the voltage inversion and the voltage inversion time. Moreover, the inversion time and the detection range are tunable by controlling the number of layers of the enzyme and through pH control of the urea-containing solution.

. Because it is possible to infer ionic behaviors at the solid-liquid interface simply by using very small amounts of water in droplets through the ionovoltaic device, the surface modification studies are essential to those seeking expansions

of research on ion dynamics at solid-liquid interfaces and various sensing applications such as biomolecules or specific ion sensors. Although we focused on the detection of urea and pH sensing in this work, we believe that the ionovoltaic can be extended to numerous application areas related to solid-liquid interface and aqueous based materials.

3.6 Experimental details

Fabrication of glass probe with urease. A 1 cm × 6 cm glass probe was used to drag water droplets and as urease attachment sites for urea degradation. The urease was attached only to the end of the glass plate in a 1×1 cm region. For the attachment of urease on the glass plate, we used a layer-by-layer (LBL) method with the opposing static charge of polyethylenimine (PEI) (branched, Mw~25000, Sigma-Aldrich) and urease (from Canavalia ensiformis (jack bean), type IX, Sigma-Aldrich). First, bare glass was treated with O_2 plasma for ten seconds at a power of 100 W. Subsequently, the glass was incubated in an aqueous solution of 5 wt% PEI for 15 min and then rinsed with distilled water, after which it was immersed in 2 mg/ml of urease in a PBS buffer solution for 30 min. In this case, the adsorption of PEI and urease was carried out three times alternately and three layers of urease were formed.

Fabrication of pH-sensitive ionovoltaic transducer. The ITO (indium tin oxide, 120 nm) on the glass was patterned with two parallel electrodes (10 mm × 29 mm) and a gap (2 mm). The pattered ITO on the glass was cleaned sequentially with a detergent, distilled water, acetone and IPA (isopropyl alcohol) in an ultrasonic bath and then dried with nitrogen gas. After the cleaning process, the ITO-coated glass was treated with O_2 plasma for ten seconds at a power of 100 W. PDMS was used as an insulating layer. An unlinked PDMS (10:1 base and cross-linker) (Sylgard-184, Dow Corning) solution was poured onto the plasma-treated substrate (ITO-coated glass). The unlinked PDMS was then spin-coated onto the pattered substrate at 5000 RPM for 1 min and annealed at 100 °C for three hours. Subsequently, the unreacted PDMS was removed with IPA, following by drying with nitrogen gas. The thickness of the PDMS film was measured with an Alpha-Step device, which indicated that the thickness was 10 μm. For the pH-sensitive surface, two materials, APTES and PFOTS, were used. The SAMs of the APTES and PFOTS were deposited using a stepwise method. First, an O_2-plasma-treated PDMS-coated substrate was immersed in 5 wt% of an APTES aqueous solution for ten minutes. After rinsing the unreacted APTES with distilled water, the substrate was dried with nitrogen gas. As a second step, the APTES-deposited substrate was placed in a sealed glass vessel

for the deposition of PFOTS. Unreacted PFOTS was then removed with IPA and the substrate was dried with nitrogen gas.

3.7. Reference

[1] S. H. Kwon, J. Park, W. K. Kim, Y. Yang, E. Lee, C. J. Han, S. Y. Park, J. Lee and Y. S. Kim, Energy Environ. Sci. 7 (2014) 3279-3283.

[2] J. Park, Y. Yang, S. H. Kwon and Y. S. Kim, J. Phys. Chem. Lett. 6 (2015) 745-749.

[3] Y. Yang, J. Park, S. H. Kwon and Y. S. Kim, Sci. Rep. 5 (2015) 15695.

[4] S. H. Kwon, W. K. Kim, J. Park, Y. Yang, B. Yoo, C. J. Han and Y. S. Kim, ACS Appl. Mater. Interfaces 8 (2016) 24579-24584.

[5] J. Yin, X. Li, J. Yu, Z. Zhang, J. Zhou and W. Guo, Nat. Nanotechnol. 9 (2014) 378-383.

[6] J. Yin, Z. Zhang, X. Li, J. Yu, J. Zhou, Y. Chen and W. Guo, Nat. Commun. 5 (2014) 3582.

[7] G. Zhu, Y. Su, P. Bai, J. Chen, Q. Jing, W. Yang and Z. L. Wang, ACS Nano 8 (2014) 6031-6037.

[8] Z. H. Lin, G. Cheng, S. Lee, K. C. Pradel and Z. L. Wang, Adv. Mater. 26 (2014) 4690-4696.

[9] S. S. Kwak, S. Lin, J. H. Lee, H. Ryu, T. Y. Kim, H. Zhong, H. Chen and S. W.

Kim, ACS Nano 10 (2016) 7297-7302.

[10] S.-B. Jeon, D. Kim, G.-W. Yoon, J.-B. Yoon and Y.-K. Choi, Nano Energy 12 (2015) 636-645.

[11] L. E. Helseth and X. D. Guo, Langmuir 31 (2015) 3269–3276

[12] J. K. Moon, J. Jeong, D. Lee and H. K. Pak, Nat. Commun. 4 (2013) 1487.

[13] Q. Liang, X. Yan, Y. Gu, K. Zhang, M. Liang, S. Lu, X. Zheng and Y. Zhang, Sci. Rep. 5 (2015) 9080.

[14] S. J. Park, K. S. Cho and S. H. Kim, J. Colloid Interface Sci. 272 (2004) 384-390.

[15] S. H. Shin, Y. H. Kwon, Y. H. Kim, J. Y. Jung, M. H. Lee, J. Nah, ACS Nano 9 (2015) 4621-4627.

[16] S. H. Shin, Y. E. Bae, H. K. Moon, J. Kim, S. H. Choi, Y. Kim, H. J. Yoon, M. H. Lee, J. Nah, ACS Nano 11 (2017) 6131-6138.

[17] S. H. Wang, Y. L. Zi, Y. S. Zhou, S. M. Li, F. R. Fan, L. Lin, Z. L. Wang, J. Mater. Chem. A 4 (2016) 3728-3734.

[18] Y. Tong, E. Tyrode, M. Osawa, N. Yoshida, T. Watanabe, A. Nakajima and S. Ye, Langmuir 27 (2011) 5420-5426.

[19] S. Watson, M. Nie, L. Wang and K. Stokes, RSC Adv. 5 (2015) 89698-89730.

[20] Y. K. Inhee Choi, Sung Koo Kang,Jeongjin Lee, Jongheop Yi, Langmuir 22 (2006) 4885-4889.

[21] H. F. Takashi Monde, Fujito Nemoto , Toshinobu Yoko, Takeo Konakahara, J. Non-Crystalline Solids 246 (1999) 54-64.

[22] H. J. Jeong, D. K. Kim, S. B. Lee, S. H. Kwon and K. Kadono, J Colloid Interface Sci. 235 (2001) 130-134.

[23] M. J. Lee, N. Y. Lee, J. R. Lim, J. B. Kim, M. Kim, H. K. Baik and Y. S. Kim, Adv. Mater. 18 (2006) 3115-3119.

[24] J. Kim, P. Seidler, L. S. Wan and C. Fill, J. Colloid Interface Sci. 329 (2009) 114-119.

[25] H. Yang and Y. Deng, J Colloid Interface Sci, 2008, 325, 588-593.

[26] S. C. Vanithakumari, R. P. George and U. Kamachi Mudali, Applied Surface Science 292 (2014) 650-657.

[27] W. Zhang, X. J. Luo, L. N. Niu, H. Y. Yang, C. K. Yiu, T. D. Wang, L. Q. Zhou, J. Mao, C. Huang, D. H. Pashley and F. R. Tay, Sci. Rep. 5 (2015) 11199.

[28] M. Yuqing, C. Jianrong and F. Keming, J. Biochem. Biophys. Methods 63 (2005) 1-9.

[29] Y. Liang, J. Huang, P. Zang, J. Kim and W. Hu, Applied Surface Science 322 (2014) 202-208.

[30] Yi Cheng, P. Xiong, Nano Lett 8 (2008) 4179-4184

[31] K. Awsiuk, A. Budkowski, A. Psarouli, P. Petrou, A. Bernasik, S. Kakabakos, J. Rysz and I. Raptis, Colloids Surf. B Biointerfaces 110 (2013) 217-224.

[32] E. H. Williams, A. V. Davydov, A. Motayed, S. G. Sundaresan, P. Bocchini, L. J. Richter, G. Stan, K. Steffens, R. Zangmeister, J. A. Schreifels and M. V. Rao, Applied Surface Science 258 (2012) 6056-6063.

[33] S. Kumar-Krishnan, A. Hernandez-Rangel, U. Pal, O. Ceballos-Sanchez, F. J. Flores-Ruiz, E. Prokhorov, O. Arias de Fuentes, R. Esparza and M. Meyyappan, J. Mater. Chem. B 4 (2016) 2553-2560.

[34] S. K. Vashist, E. Marion Schneider, E. Lam, S. Hrapovic and J. H. Luong, Sci. Rep. 4 (2014) 4407.

[35] K. Spencer, Ann Clin. Biochem. 23 (1986) 1.

[36] E. Prats-Alfonso, L. Abad, N. Casan-Pastor, J. Gonzalo-Ruiz, E. Baldrich, Biosens. Bioelectron. 39 (2013) 163

[37] M. Singh, N. Verma, A. K. Garg, N. Redhu, Sensor Actuat. B-Chem. 134 (2008)

345.

[38] X. Chen, Z. P. Yang, S. H. Si, J Electroanal Chem. 635 (2009) 1

[39] C. Eggenstein, M. Borchardt, C. Diekmann, B. Grundig, C. Dumschat, K. Cammann, M. Knoll, F. Spener, Biosens. Bioelectron. 14 (1999) 33

[40] B. A. Petersson, Anal. Chim. Acta 209 (1988) 239.

[41] Tiwari, S. Aryal, S. Pilla, S. Q. Gong, Talanta 78 (2009) 1401

[42] P. Bertocchi, D. Compagnone, G. Palleschi, Biosens. Bioelectron. 11 (1996) 1

[43] F. Kuralay, H. Ozyoruk, A. Yildiz, Sensor Actuat. B-Chem. 114 (2006) 500.

[44] W. Limbut, P. Thavarungkul, P. Kanatharana, P. Asewatreratanakul, C. Limsakul, B. Wongkittisuksa, Biosens. Bioelectron. 19 (2004) 813.

[45] W. Y. Lee, S. R. Kim, T. H. Kim, K. S. Lee, M. C. Shin, J. K. Park, Anal. Chim. Acta 404 (2000) 195

[46] M. M. Castillo-Ortega, D. E. Rodriguez, J. C. Encinas, M. Plascencia, F. A. Mendez-Velarde, R. Olayo, Sensor Actuat. B-Chem. 85 (2002) 19.

[47] E. Piecinini, C. Bliem, C. Reiner-Rozman, F. Battaglini, O. Azzaroni, W. Knoll, Biosens. Bioelectron. 92 (2017) 661.

[48] C. Puig-Lleixa, C. Jimenez, J. Alonso, J. Bartroli, Anal. Chim. Acta 389 (1999)

179

[49] G. O. Silva, M. Mulato, ECS J. Solid State Sc. 7 2018 Q3014.

[50] N. F. Starodub, A. V. Rebriev, Bioelectrochemistry 71 (2007) 29.

[51] J. Park, S. Song, Y. Yang, S. H. Kwon, E. Sim, Y. S. Kim, J. Am. Chem. Soc. 139 (2017) 10968

[52] Y. Yang, J. Park, S. G. Yoon, Y. S. Kim, Nano Energy 40 (2017) 447.

[53] J. Park, S. Song, C. Shin, Y. Yang, S. A. L. Weber, E. Sim, Y. S. Kim, Angew. Chem. Int. Edit. 57 (2018) 2091.

Chapter 4 Structural Engineering of Ionovoltaic Device and Applications

4.1 Introduction

In this chapter, a clear understanding of the working mechanism of the ionovoltaic device is studied through the overall structure and electrode engineering. Especially, the device structure which was performed in the flat plate with flowing or squeezing droplets was modified by applying fluidic channel with sequencing flow with air slug and water droplet, and the device which continuously generated electricity through the mono-electrode development was studied and the electron flow mechanism was identified.

4.2 Fluidic ionovoltaic device

Flows in small size channels or tubes can usually be seen in nature, daily life and technology. For example, blood vessels in our body, the phloem and xylem in plants, and ground water in soil spaces or cracks are commonly found flows in nature. Artificially, we also see flows in channels or tubes not only in daily life like water lines in a purifier or heat exchanger but also in technology

advancements such as lab on a chip technology, fluidic electronics and water cooling systems in high power electronics. These various flows in small channels and tubes have potential as a source of energy. For flows in small channels as an energy source, many researchers have studied not only the diverse and abundant sources in nature and daily life but also integration capability[1] and applicability to the fields of biology[2], medical[2-4] and chemistry[5].

Specially, interest in electricity generation with flows in a channel has been recently increased in the fields of micro energy harvesting and sensing [6-10]. Several techniques such as variation of capacitance [6, 7], reverse electro-wetting [8] and electro kinetic flow [9, 10] have been studied. However, there are several drawbacks to the variation of capacitance and reverse electro-wetting techniques, which are the necessity of external sources such as a bias voltage or pre-charging processes to maintain a voltage difference in capacitor [6-8]. The energy generation of electro kinetic flows uses a pressure gradient in nano-sized channel arrays as a streaming potential [9-10], which need complicated fabrication processes such as a micro- or nano-patterning process for nano-channel arrays. These challenging points still remain for many applications of electricity generation using flows in a channel.

Recently, we reported on an active transducer for effective electricity generation

via various water motions without any bias voltage sources [11, 12]. Based on this concept, herein, we propose a new fluidic electricity generator (FEG) by modulating the electric double layer (EDL) with two phase flows of water and air without any external power source. The driving force of electricity generation in the FEG is that the ion dynamics, which are induced by motion modulations between electrodes and water, make an electricity. To verify the assumption, electric signals between two electrodes of FEG were checked for various water/air passing conditions, such as entering and leaving on channels, and passing into channels with different lengths. Moreover, we verified the possibility of a self-powered air slug sensor by applying the FEG in the detection of an air slug.

4.2.1 Fabrication method and device performance

The schematic and photograph (inset) images of the FEG are shown in [Fig. 4.1a]. A sandwich structure of electrode / PDMS / electrode was adopted for the FEG. Two types of PDMS channels 18 mm and 36 mm long were fabricated with a 2 mm × 1.9 mm^2 cross-section in both. The top electrode consisted of ITO glass as an electrode, P4VP (poly 4-vinyl phenol) as a dielectric layer and a silica gel layer that included PFOTS as a hydrophobic layer. Each layer was spin-coated

and baked at 200 °C. For the bottom electrode, only silica-gel film that included PFOTS was coated on the ITO glass by spin coating. The details of the experimental conditions are explained in the experimental details. The PDMS channel mounted with two electrodes was closed by a three prong clamp and connected to the PTFE tubes with 1.6 mm inside diameter. An inlet tube was connected to the segmented sequences of the water/air generating system, and an outlet tube was connected to a syringe pump. All the flows were operated in the suction mode of the syringe pump. Both the top and bottom electrodes were connected to measuring equipment as shown in the schematic image of [Fig. 4.1b]. [Fig. 4.1c, d] shows the measured output voltages and currents while the two phase sequences consisted of a 10 cm column of 0.01 M NaCl water solution and 30 cm air slide continuously in the FEG at a flow rate of 30 ml/min. The positive voltage and current signals were measured when the head of a water column moved into the channel, and negative signals were measured when the tail of a water column left the channel. The peak to peak voltage and current were ~0.19 V and ~0.331 μA, respectively.

[Fig. 4.2a] explains the working mechanism of electricity generation in the FEG. The driving force of electricity generation in the FEG is assumed to be EDL modulation at the interface between the transducer and water [11-13]. When the

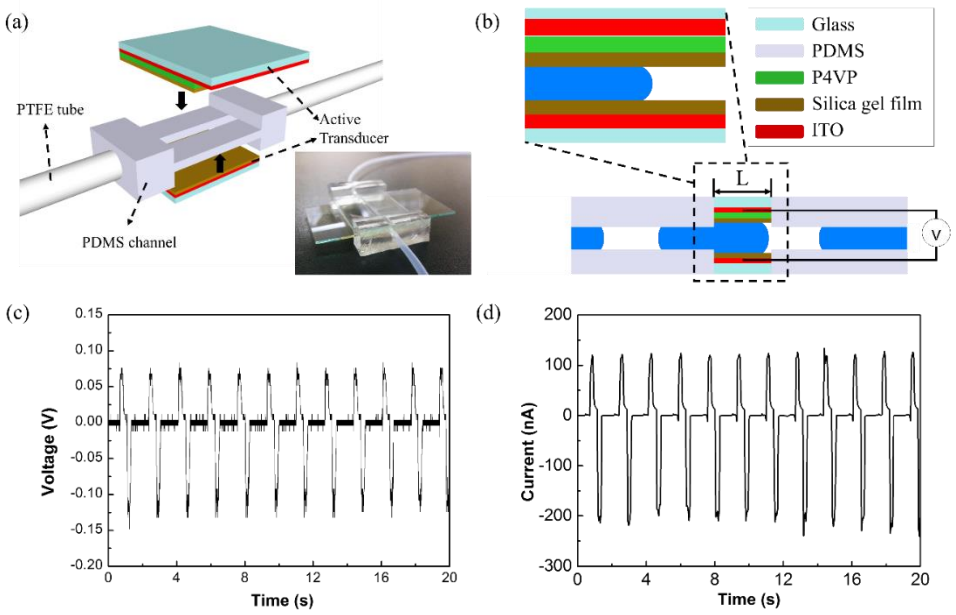

Figure 4. 1 (a) Schematic image and photograph of the FEG. (b) Side view of the FEG which includes the PDMS channel, water/air, and components of the active transducer. L is the length of the channels (L: 1.8 cm and 3.6 cm). (c) The measured output voltage and (d) current of the FEG with 10 cm of 0.01 M NaCl water solution and 30 cm air sequence flowing through a 3.6 cm length channel. The two phases of water and air had a flow rate of 30 ml/min with a syringe pump.

0.01 M NaCl water solution contacts the top and bottom electrodes, cations are adsorbed at the top and bottom electrodes. Electrons and counter ions come near to the electrodes' surface for charge neutralization. At that time, the cations are asymmetrically adsorbed by the silica-gel coated P4VP film in the top electrode in the FEG [11, 12], and the electrons flow through the external circuit, which generates electric currents. In the case of water leaving, the reverse process occurs in which the adsorbed ions are detached by the mechanical motion of the water column. The hold electrons by cations return through the external circuit and generate reverse electric currents. For electricity generation in the FEG, the voltage difference between bottom electrode and ground was almost zero. This result indicates that few electrons were induced by the cations at the bottom electrode, [Fig. 4.2] and the effects were negligible. Therefore, the voltage difference between the top and bottom electrodes can be expressed as $V_T = d\left(\frac{Q_T}{C_T}\right)$ [Fig. 4.3], where C_T is the capacitance of the EDL which is formed between the top electrode and water and V_T is the voltage on C_T. The charge Q_T can be expressed by multiplying C_T and V_T. In this equation, the variation area of the EDL is an important factor for electricity generation. It means that the flow of the charges is induced by increasing/ decreasing the contact area between the water and the silica-gel coated P4VP film on the top electrode. To verify this

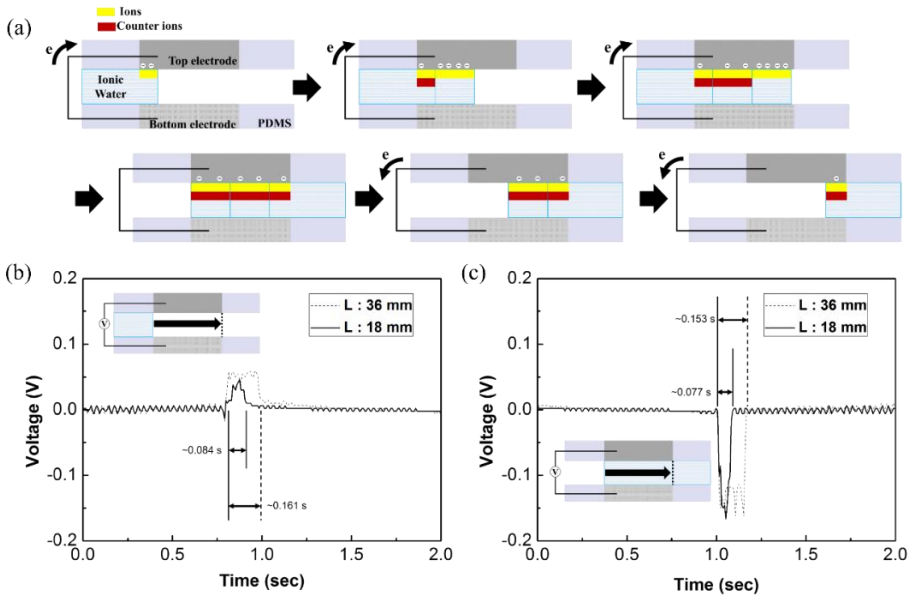

Figure 4. 2 (a) Basic mechanism of the FEG. Yellow layer is the attracted ions and red layer is the counter ions. (b) Positive voltage signal was measured when the head of a water stream moved into the channels and (c) negative voltage was measured when the tail of a water stream left the channels. The measured output voltage for the 18 mm and 36 mm length channels with a water stream flow rate of 30 ml/min are represented by the red and blue lines, respectively.

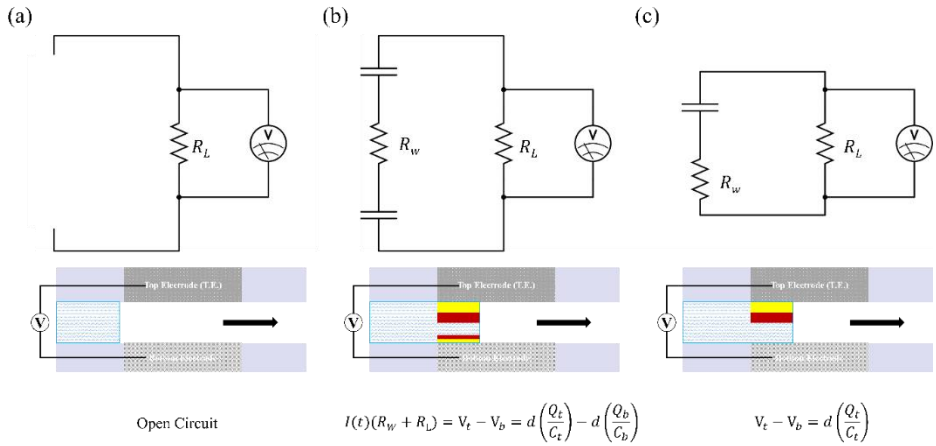

Figure 4. 3 The total system is an open circuit until the water column comes into contact with the top and bottom electrodes (a). With the contact of the water and electrodes, the circuit is shorted, and EDLs are formed at the top and bottom electrodes (b). At that time, voltage difference follows the equation10 shown in (b), where RW and RL are the resistance of the water and circuit like the voltmeter and wires; Vt and Vb are the voltages on Ct and Cb. The bottom electrode effect is small enough to be negligible. Thus, the voltage difference can be expressed as the equation shown in (c).

assumption, the holding time of the voltage difference between the top and bottom electrodes were checked when the water was passing through the channels which have different lengths. According to the hypothesis, the voltage difference should be maintained while the water column passes through the FEG channel. Therefore, the time it takes for the water column to pass through the different lengths of channels should be different. [Fig. 4.2b, c] shows the measured output voltage versus time. The dash line is the measured voltage data at a flow rate of 30 ml/min for the 3.6 cm long channel when the water went in and out. The solid line represents the voltage data for the 1.8 cm long channel. The voltage maintenance time when the head of the water entered for the long channel case was ~0.161 s and for the short channel case was ~0.084 s shown in Figure 2b. When the tail of the water column left the channels, the maintenance time was ~0.153 s and ~0.077 s for the long and short channel, respectively. When the water column went in and out with same pressure applied, more time was required to reach the end of the active transducer in the longer channel shown as the dotted line on the inset images of [Fig. 4.2b, c]. These results indicate that the flow of charges was induced by increasing/decreasing the contact area between the water and silica-gel coated P4VP film on the top electrode in the FEG.

The maintenance voltage signals were measured like a noise. The 17.9, 26.9 %

of voltages variations measured during the voltage differences maintained when the water went in and out for the 3.6 cm long channel at a flow rate of 30 ml/min. This signals come from irregular water motions because the width of the channel is not

perfectly uniform. The residual layers at the side of the channel are from the PDMS channel fabrication step which induces a little fluctuation in the water. For that reason, the irregularity of wetting and dewetting occurred intermittently in the channel, which causes a fluctuation in the signals.

The FEG was tested as an energy harvester with a two phase flow. [Fig. 4.4a] shows the output power when multiple water columns flowed through the FEG. A 2.2 MΩ external road resistor was used to measure power. There were two peak power signals per cycle shown in the data of [Fig. 4.4a]. As the water columns entered the channel case, the measured power was ~1.22 nw and ~7 nW as the water columns left the channel. The average peak power was ~5.64 nW with 10 cm long water and a 30 cm air sequence with a flow rate of 30 ml/min. ~0.94 nJ per water column was measured inset image in [Fig 4.4a]. [Fig. 4.4b] shows that the output voltage and power depended on the velocity of the water columns. The voltage and power increased with an increasing flow rate of the water column. It means that the larger variation of the contact area per second induces higher

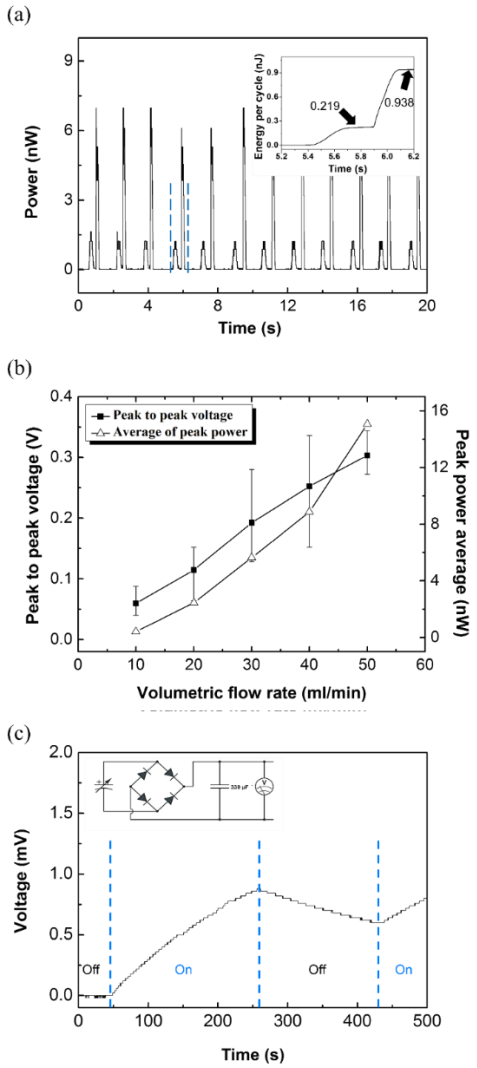

Figure 4. 4 (a) shows the output power when multiple columns of water (10 cm) and air (30 cm) moved with a volumetric flow rate of 30 ml/min. Inset plot shows the generated energy per a cycle. (b) The measured peak to peak voltages and peak power averages at different volumetric flow rates. (c) The voltage data from a storage circuit (inset) containing a capacitor and a full wave rectifier.

power and energy. The inset image of [Fig. 4.4c] shows a simple energy storage circuit containing a full wave rectifier and a 330 μF capacitor. The voltage of the capacitor was monitored with a voltmeter while multiple water and air sequences passed through the FEG for 560 s. The same conditions of length of the water and air in the output power experiment were used in the charging experiment. The capacitor was fully discharged before the test (Fig. 4.4c, zone 1). During the operation of the FEG, the output voltage increased

4.2.2 Application of ionovoltaic device as an air-slug sensor

Two phases of water and air flow are widely used in various fields such as the cooling systems of high power electronics, medical devices [14] and micro reactors [15] for chemical analysis because the flows have high mass and heat transfer rates in tubes and micro channels [16, 17]. In these applications, the slug length and speed of the segmented flow have very important roles that affect the mass and heat transfer between phases. A monitoring device for slug length and speed is a necessary part of a two phase flow adopted system, and optical [18, 19] and electrical methods [20, 21] have been suggested as monitoring systems for segmented flow. With this in mind, we checked the possibility of using the proposed FEG as a self-powered air slug sensor. For the sensing test, a 3.6 cm long FEG, air slug, and 0.01M NaCl solution were used. To verify the velocity of

the slug flow, captured images from a high-speed video camera (MotionPro x4TM, Imaging Solutions GmbH) were used. The length of the air gap between the water columns prepared was 12 cm long (0.2616 ml), and the volumetric flow rate was 30 ml/min. [Fig. 4.5a] shows the output voltage and the divided five zones (A~E) according to distinctive features when the air gap and water stream passed through the FEG. At zone A, there was no potential difference between the top and bottom electrodes because the FEG channel was filled with the first water column and just flowed without any variation in contact area. When the head of the air slug (tail of the first water column) entered the FEG channel [Fig. 4.5b, c], a decrease in the contact area between the water and FEG caused a negative peak shown in Figure 4a, zone B for several milliseconds. Zone C had no signal because of the passing region of the air slug. When the head of the second water stream (end of the air slug) approached the channel [Fig. 4.5d, e], a positive peak was measured (zone D) because of the formation of the contact area between the second water column. There was no signal in zone E for same reason as in zone A. Zones A, B and C provided information on the slug length and velocity of flow. The velocity of flow

was easily estimated from the measured voltage difference at zones A and C. Peak to peak voltage from the self-powered sensor was ~0.201 V, and this value

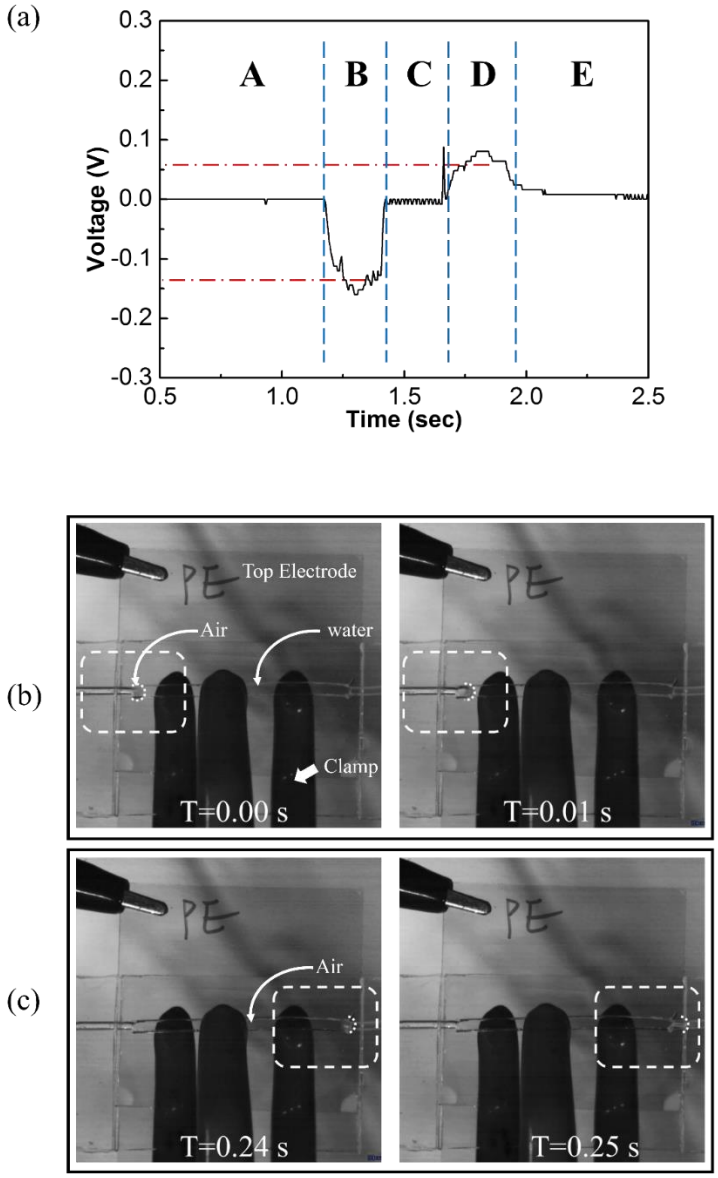

Figure 4. 5 (a) shows application of the FEG for a segmented flow sensor with a two phase flow. (b), (c) High-speed camera images of the flowing water column from top view.

is almost similar to the value (~0.19 V) for the volumetric flow rate of 30 ml/min. Therefore, the velocity of the flow was 13.16 cm/s which was converted from the volumetric flow rate to velocity in a channel which has a 2 mm × 1.9 mm cross sectional area. The length of the air slug was calculated by multiplying time by flow velocity. The

times at zones B and C (0.503 s) provide the total length of the air slug. It was calculated as 6.61 cm at the cross sectional area of the channel with a total volume of ~0.25 ml which is acceptable data compared to 0.2616 ml. To verify, the velocity of the flow was measured from the frame numbers of the high speed movie which was recorded at 100 frames per 1 second. Twenty-six frames were captured, and this means that it took 0.26 s for the head of the air slug passing through the channel [Fig. 4.5b, c]. From the time information, the velocity of the flow was measured as 13.8 cm/s and the calculated velocity of 13.16 cm/s from the self-powered sensor was reasonable. Although several factors were not considered in this experiment such as the friction between the water and the tubes and air gap compression at the channel, from these results, we successfully verified that FEG can be used as a self-powered slug detector in a small fluidic channel.

4.3 ITO mono-electrode based ionovoltaic device

Recently, a transducer research has been actively conducted to produce electricity through contact with the ionic water and has achieved a great deal of accomplishment in principle analysis [12, 25] and applications [11, 26-30]. In particular, transducers using EDL (electrical double layer) modulations, such as ion adsorption and desorption, are attracting attention because of their advantages in eco-friendly, simple drive systems and self-powered characteristics. In the most studies, two parallel electrodes were used to instantaneously measure the potential difference between the front and the rear of the water droplet, or by pressing / releasing the water droplet, the area difference of the EDL of the part in contact with the transducer was used [11,31,32]. However, since the electric signals appear in the form of pulses, they are inevitably low in terms of energy density, and it is difficult to analyze phenomena occurring at the solid-liquid interfaces.

In order to overcome these limitations, researches have focused on the transducer that generates electric signals throughout the water droplet rolling by adjusting the material and resistance of the mono-electrode. For example, in mono-electrode studies using graphene, the origin of the electrical signal that the ion dynamics by the polarity of solid surface has been revealed and it has

demonstrated its utility as an energy harvesting device [33,34]. In recent research, a transducer has been reported that produce electricity from water movements such as waves using sputtered ZnO mono-electrode [35].

In our previous work, a high-resistance silicon wafer was applied as an electrode of the transducer to investigate the operating principle of the device named as an ionovoltaic transducer and derive the dominant characteristic equation [eq. 2.1]. The ionovoltaic device generates electricity due to the change of electron density by adsorption (front of droplet) and desorption (rear of droplet) of ions at the solid-liquid interface when an ionic water droplet flows on the device [25]. Therefore, interestingly, this device uses a resistor with a relatively high resistance as an electrode for the maintaining of the potential difference between the front and the rear of the droplet, unlike conventional electronic devices. For the ionovoltaic device that has such a resistive characteristic and produces an efficient electricity, a proper range of resistance value is required such that the electrode should not be short-circuited or opened while maintaining a potential difference.

Because the resistive band can be easily adjusted through precursor control or process variable control in fabrication steps, in this particular region of resistance, a metal oxide is a suitable material for analyzing the role of resistance in the

ionovoltaic device. In the typical factors that determine the resistance of the oxide semiconductor electrode are divided into the grain boundary and the resistance element in the bulk such as oxygen vacancy (carrier concentration and mobility), but the influence of each factor on the ionovoltaic device has not been studied sufficiently. Indium tin oxide (ITO) is a n-type semiconductor with wide bandgap of ~4eV that can control the grain boundaries and oxygen vacancies through control of sputtering process parameters [37,38]. Therefore, ITO can be a good candidate as a high-resistance semiconductor electrode for ionovoltaic device to explore the relationship between resistance and electric performance, as well as the quest for conduction mechanisms in ionovoltaic transducers.

In this study, we investigated the effect of grain boundary and oxygen vacancy on the properties of ITO based ionovoltaic device through analysis of relationship between resistance and output performance. We have been able to understand a little more about the driving principle of the device which is not clarified through this study, and to predict the characteristics of the optimized device. Especially, when the ITO film is deposited by sputtering system, the resistance can be controlled by various parameters such as the type of a substrate, power control, distance adjustment from the target, pressure control, types and flow rate of the gas, and the post process. Among them, the ITO electrodes resistances for the

ionovoltaic transducers were adjusted by working pressure(P_{Ar}), and oxygen partial pressure(P_{Ar+O2}) in the chamber and the compared the electrical characteristics as an ionovoltaic transducer in each case. In addition, due to the sputtering process and inherent characteristics of amorphous ITO, the possibilities of scale-up and patterning of transparent bendable ITO-based ionovoltaic device were verified.

4.3.1 Fabrication of ITO mono-electrode and ionovoltaic device

Deposition of indium tin oxide films. Table 4.1. shows ten samples according to the working pressure (P_{Ar} | OW, W1, W2, W3, W4) and oxygen partial pressure (P_{Ar+O2} | OW, O1, O2, O3, O4) during deposition process of the ITO. The ITO was sputtered on the glass substrates by a DC magnetron sputtering system using an indium tin oxide (In_2O_3:SnO_2=9:1wt%) target under ~30 W of sputtering power at room temperature. In case of the adjust of working pressure, the working pressures of the ITO were controlled by 24 SCCM of Ar gas and varied from 2 mTorr to 50 mTorr. In case of the control of oxygen flow rate, the working pressure was fixed with 2 mTorr and the flow rates of oxygen were adjusted from 0.0 to 0.8 SCCM by the unit of 0.2 SCCM under 24 SCCM of Ar maintained. The thickness of all samples were 40 nm thickness.

Fabrications of the ionovoltaic transducer. After ITO deposition process, the

as-deposited ITO mono-electrodes were coated *via* spin coating method with silica gel film containing PFOTS under 3500 rpm for 60 seconds and annealed at 150 ℃ for 20 min. Thickness of silica gel film was measured with alpha step and it was about 300 nm.

Characterization of the fabricated devices. The output characteristics were measured using Keithley 2182A nanovoltmeter and 6485 picoammeter, respectively. The two-wire (distance 6 cm) resistance of the ITO were measured with Keysight B2902A. Thermo Fisher Scientific K-Alpha+ X-ray photoelectron spectrometer (XPS) was used to measure the oxygen ratio at the surface of the ITO samples.

Temp.	*R.T.*	
Power.	*27W*	
Thickness	*~ 40 nm*	
Sample No.	***Working Pressure (mTorr)***	***P_{O2} (SCCM)***
OW	2	0.00 (0)
O1		0.83 (0.2)
O2		1.64 (0.4)
O3		2.44 (0.6)
O4		3.23 (0.8)
W1	10	0.00 (0)
W2	20	0.00 (0)
W3	30	0.00 (0)
W4	40	0.00 (0)
W5	50	0.00 (0)

Table 4.2 Sputtering condition for ITO mono-electrode of ionovoltaic device

4.3.2 Influence of sputtering parameters on a characteristics of ITO mono-electrode based ionovoltaic device.

A photograph and schematic images of ITO mono-electrode based ionovoltaic transducer (IMIT) (O4 smaple) are shown in [Fig. 4.6a]. The IMIT is transparent and have high contact angle (~103°). The output voltage of 120 mV and current of 35 nA were continuously generated when the 10 mM of NaCl droplet (150 microliters) was flowed at 5 cm/s on the IMIT [Fig. 4.6b]. Converting the IMIT and the water droplet into an equivalent circuit is shown in Fig. 1c. As the droplet flows, adsorption and desorption of ions take place at the front and rear of the droplet, which can be expressed as the capacitors C_f and C_b, respectively. In this case, the resistance R_p which is the resistance of the overlapped part of the ITO electrode with the water droplet for maintaining the potential difference of the C_f and C_b becomes a key factor. Because high conducting electrodes balance the potential difference due to adsorption and desorption of the cations at the liquid-solid interface too quickly, an electrode of appropriate resistance in required for the performance of the transducer. Therefore, the proper range of resistance was investigated by the sputtering process under the varied working pressure and oxygen partial pressure that the mono-electrode was not shorted or opened. In the case of the working pressure (P_{Ar}) control in the sputtering system, the kinetic energy of the bombarded ITO particles reaching the substrate is reduced by the

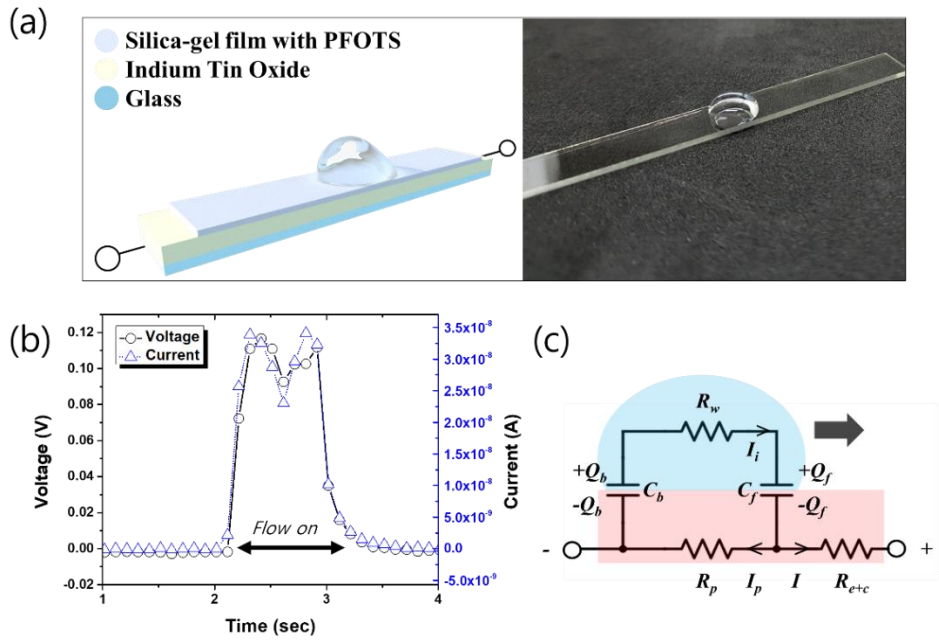

Figure 4. 6 (a) Schematic and photograph images of ITO mono-electrode based ionovoltaic device. (b) Output performance of the device (sample O4) with 10 mM of Nacl droplet and 5 cm/s of droplet speed. (c) Equivalent circuit of the ionovoltaic device and water droplet.

high gas pressure in the chamber, and the particle size forming the thin film is reduced. The 40 nm of ITO films deposited at the low P_{Ar} exhibit a compact morphology as shown in sectional SEM image of [Fig. 4.7a]. However, in the case of ITO deposited at high P_{Ar} [Fig. 4.7b], grain boundaries were formed due to the columnar growth of ITO. In other words, at a condition of high P_{Ar}, more grain boundaries are generated and it plays a decisive role in raising the overall resistance of the electrode [36]. The higher the P_{Ar}, the greater the overall resistance of the ITO electrode, which is consistent with previously reported studies. To investigate the influence of the resistance which derived from grain boundaries of columnar ITO on the electrical properties of ionovoltaic transducer, the output performances were tested. The IMIT was fabricated by spin coating and annealing process with the silica gel film contained PFOTS immediately after the sputtering deposition. When the 0.1 mM of NaCl water droplet flows with 5 cm/s speed on the ITO based ionovoltaic transducer, the output voltage and current were continuously generated. As the resistance of the ITO mono-electrode increases, the output voltages increase. As the ITO is deposited at high P_{Ar}, the resistance R_p increases and the potential difference between the front and rear of the droplet increases.

This result showed that the resistance of the electrode was controlled by grain

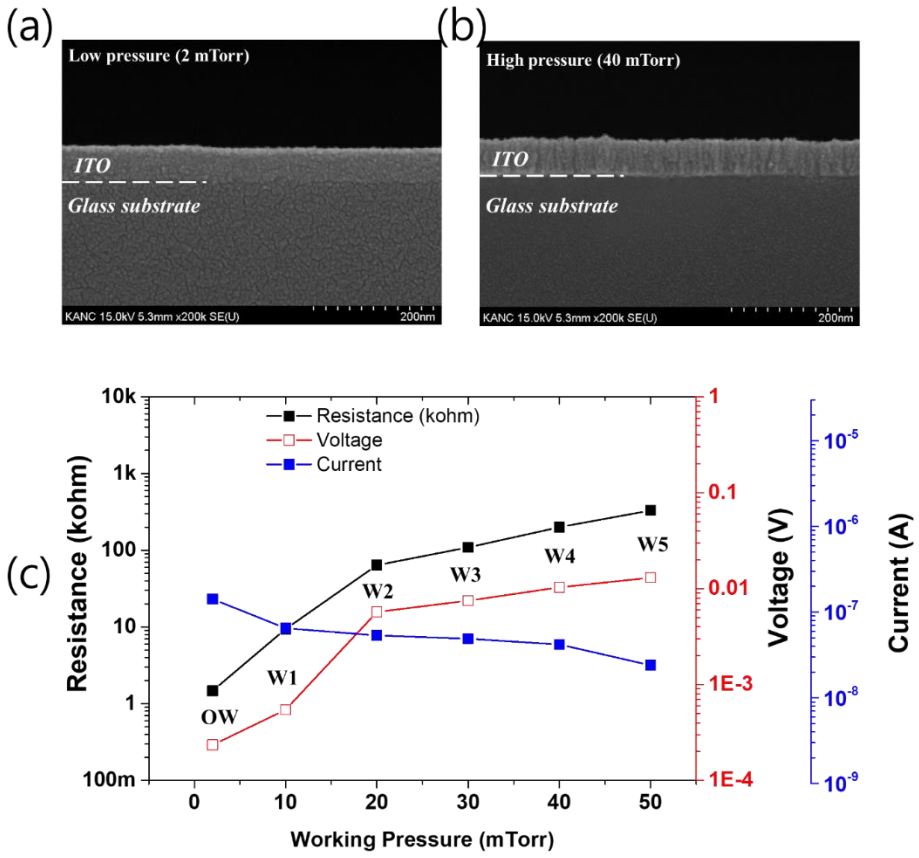

Figure 4. 7 Sectional SEM images of ITO electrode (60 nm) deposited under (a) low (2mTorr) and (b) high (40 mTorr) pressure without oxygen. (c) Output performances and resistance of the ITO based ionovoltaic device (P_{Ar} controlled devices).

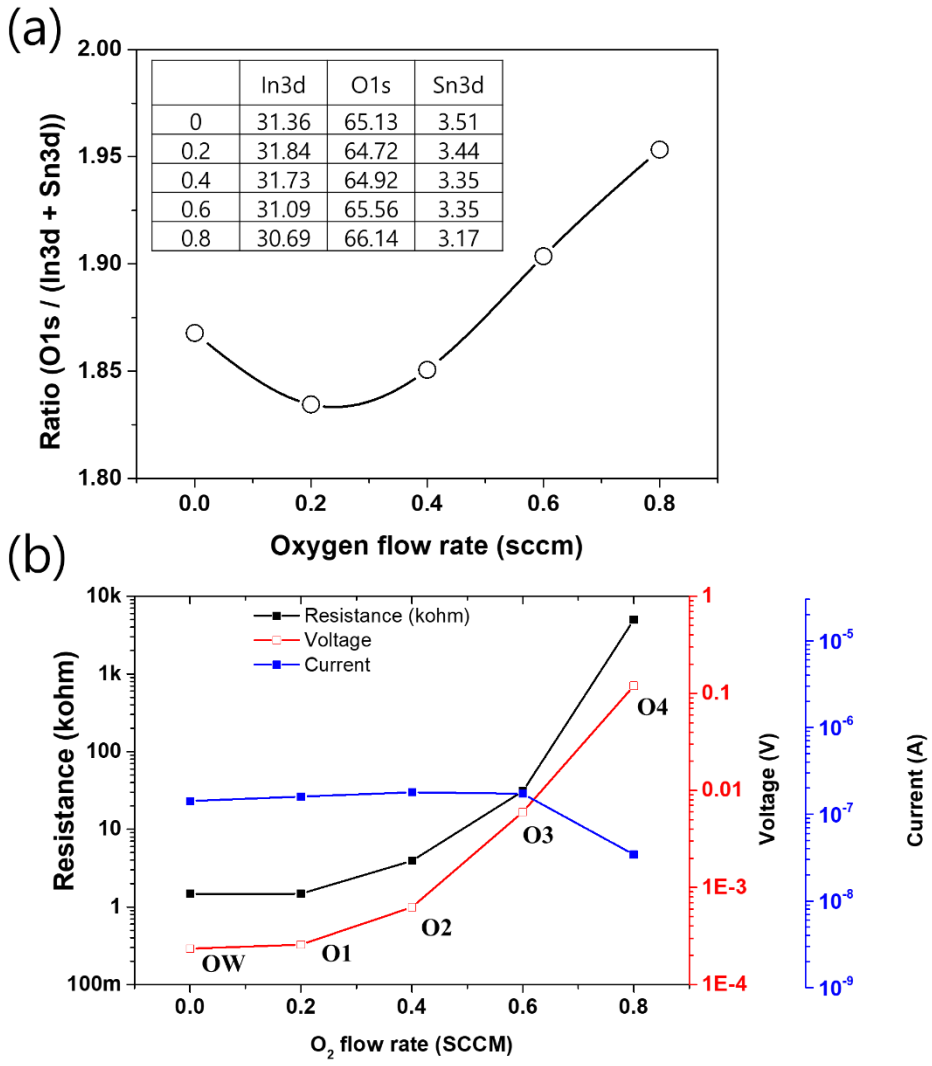

Figure 4. 8 (a) The oxygen ratio in the ITO electrodes and (b)output performances and resistance of the ITO based ionovoltaic device (P_{Ar+O2} controlled devices).

boundaries through the working pressure and that the IMIT which has the electrode deposited at the higher working pressure gave better output performances. But we do not think this is the highest performance of the device made with grain boundary adjustment. Because of the limitations of sputter chambers and throttle valves, we were only able to produce this level of resistance. However, we believe that an optimized transducer can be fabricated through process set-ups that can produce more grain boundaries for the raising resistance.

On the other hand, the resistance of the electrode adjusted by controlling the partial pressure of oxygen (P_{Ar+O2}) at a low working pressure (2 mTorr) to reduce the grain boundary and to confirm the effect of defect scattering in the bulk. In this case, the resistance of the entire electrode is controlled through the adjustment of the stoichiometric defects such as oxygen vacancies (acting as electrical carrier) inside the thin film. When oxygen is added with Ar during the sputtering deposition process, the oxygen vacancies are replaced by oxygen and the free electrons are reduced[37-39]. As a result, the overall carrier concentration is reduced and the resistance of the entire electrode is increased. During the deposition process under 2 mTorr of working pressure with 24 SCCM of the Ar flow rate, oxygen was injected and the flow rate of oxygen was increased from 0 to 0.8 SCCM in increments of 0.2 SCCM units.

As the oxygen partial pressure increases, the resistance of the ITO mono-

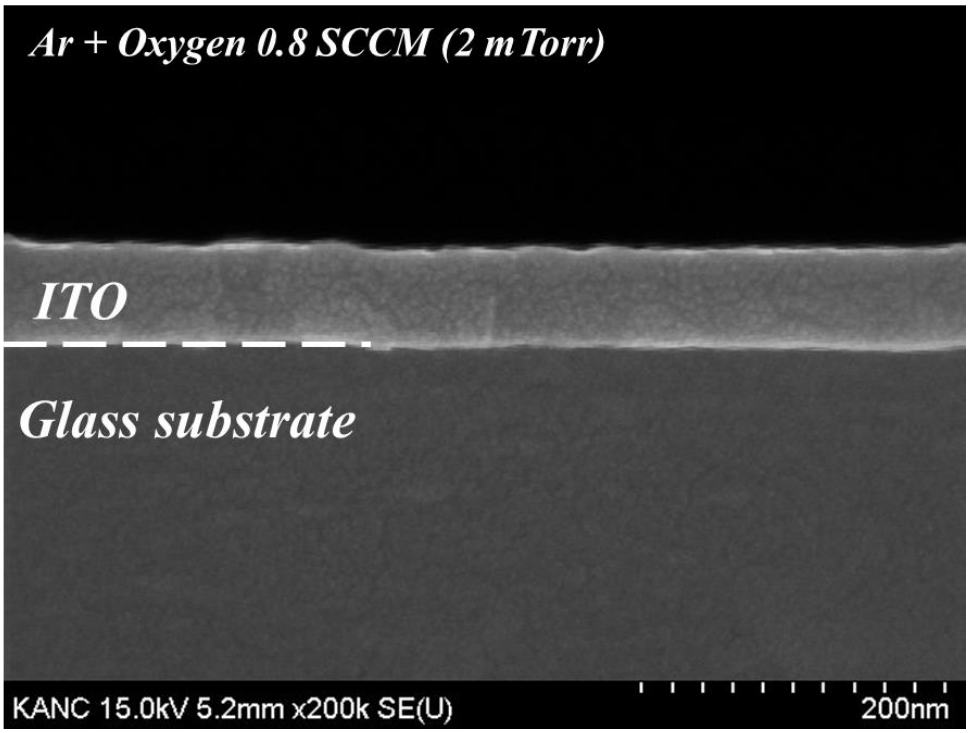

Figure 4. 9 Sectional SEM images of ITO electrode (60 nm) deposited under (a) low (2mTorr) pressure with 0.8 SCCM of oxygen.

electrode tends to increase [Fig. 4.8b]. As shown in the SEM image [Fig. 4.9], the ITO thin film is well formed without a columnar shape under the high P_{Ar}. The cause of the increase in resistance by the partial pressure of oxygen is due to the change of the oxygen vacancy. The higher oxygen content in the ITO thin film means that the oxygen vacancy decreases and the carrier concentration decreases [39]. As can be seen from the XPS data in [inset table in Fig. 4.8a], the oxygen ratio in the ITO electrode increases according to the oxygen flow rate increases. [Fig. 4.8b] shows that the ITO electrode growth from partial pressure of high oxygen flow rate has a high resistance. Because of the reduction of the carrier concentration due to the reduction of the oxygen vacancies. In addition, the peak shift of XPS spectra of In3d, Sn3d, and O1s for ITO samples with various fabrication conditions to a lower binding energy exhibit the increase of ITO work function. These results are consistent with other studies reported previously [40]. In order to verify the performance of IMIT fabricated by the P_{Ar+O2} control, after the deposition process, the as-deposited ITO electrodes were coated with the silica gel film contained PFOTS and annealed. As shown in [Fig. 4.8b], as the resistance of the IMIT increases, the output voltage generated increases. When the flow rate of oxygen is 0.8 sccm, it shows that the resistance and output voltage were the highest. The output performance is about 120 mV

when water droplets flow at 5 cm/s using 10 mM of NaCl droplet. This tendency is due to the higher resistance R_p and better maintains the potential difference generated during the adsorption and desorption phenomenon that occur at the front and rear of the droplet. Unlike the case of P_{Ar} control devices, the output current is kept constant and the current begins to decrease slightly when the circuit starts to open above a certain resistor range.

As can be seen from these results, the resistance control for the investigate the effect on the device characteristics were successfully conducted by boundary scattering and defect scattering control by sputtering process modulation. First, for working pressure control, the resistance of the electrode is adjusted by the grain boundaries, and second, the control of oxygen flow rate increases the resistance by the reduction of the carrier concentration. In both cases, the output voltage increases as the resistance of the electrode increases. The device through oxygen flow rate control has slightly higher output voltage than the voltage of the device using working pressure control [Fig. 4.10a]. This is presumably because of the more current lost in grain boundary scattering in the electrode. Taking these results into consideration, the factors that determine the resistance, and electron flows by the adsorbed ions in the IMIT can be represented as the schematic images shown in [Fig. 4.10b].

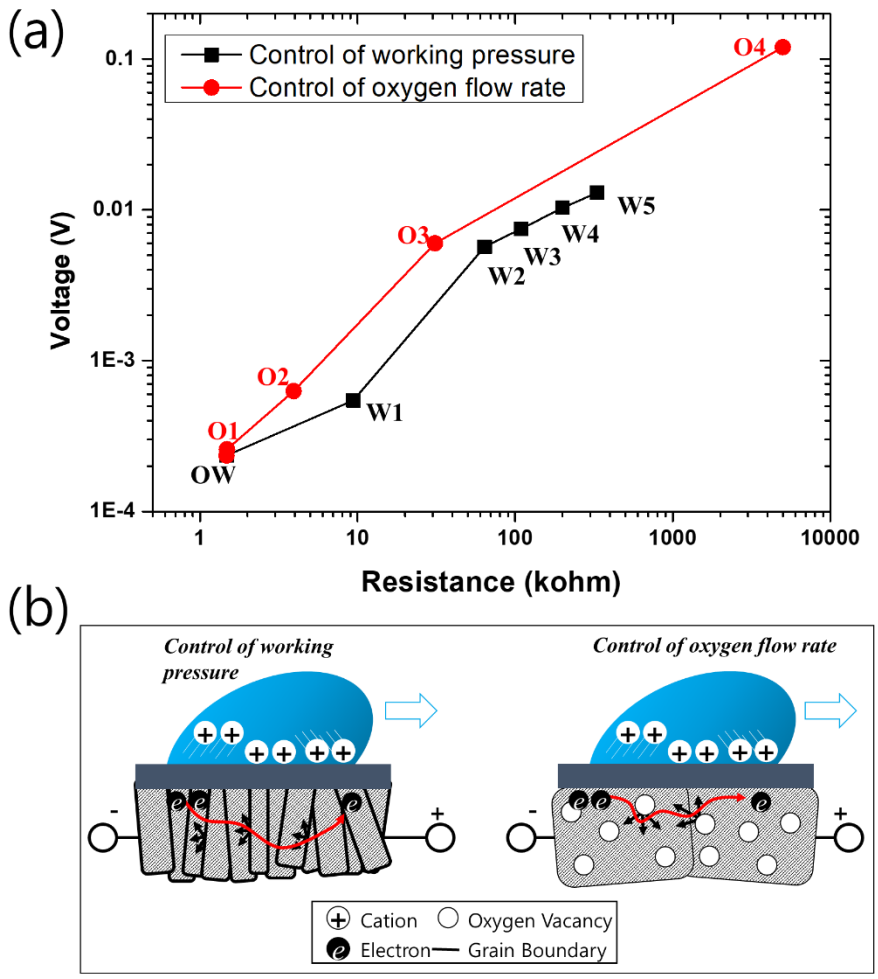

Figure 4. 10 (a) The output voltages on the resistance of IMITs and (b) schematic image of induced current by the water droplet in ITO mono-electrodes

4.3.3 Application and advantages of ITO based ionovoltaic device

In the case of the IMIT, there is a great possibility of various applications due to the sputtering process, the transparent and amorphous characteristics. It is easy to scale-up because the ITO based transducer is made by sputtering deposition and spin coating process. In addition, since the electrode can be patterned using a mask during the sputtering process, the required shape of electrode can be easily realized [Fig. 4.11a]. The amorphous electrode made of very small particles means that it is bendable depending on the type of substrate. At the sample O4 conditions, an ITO electrode was deposited on a PET film at 60 nm thickness and an ionovoltaic transducer was fabricated through spin coating with silica gel film containing PFOTS as shown in [Fig. 4.11b]. The bent IMIT was tested for its applicability as a flowing-direction sensor. As shown in [Fig. 4.11c], the sign of the measured output voltage indicates the direction of the water droplet flowing left or right. These results show that the transducer works well in bent conditions. Although we have demonstrated a very simple directional sensing application here, but because of its many advantages such as ease of scale-up, transparency, patternability and bendability, the IMIT has a great possibility for applications such the energy harvesters that can be used on the windows of buildings and vehicles and the sensors.

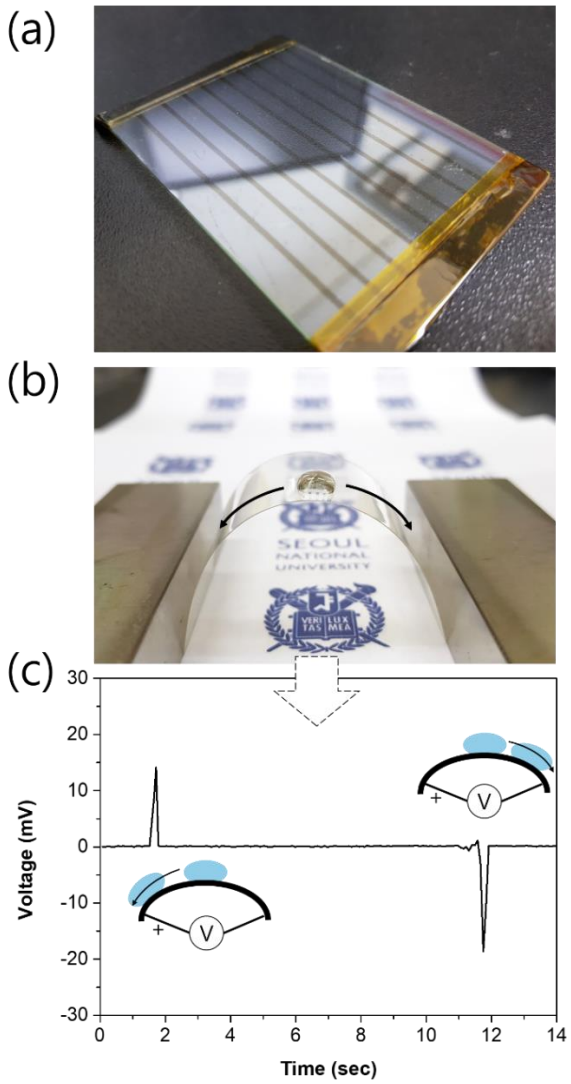

Figure 4. 11 (a) The scale-up and patterning abilities of sputtered ITO based ionovoltaic device. (b) Bendability of the ITO based ionovoltaic device and (c) demonstration in a bent state.

4.4 Conclusion

In this chapter, through structural engineering of ionovoltaic device, we were able to investigate the cause of electricity generation and succeeded in modulating electricity generation time. until now, most of the electricity generators have been water vibrational generators [22-24] but FEG (fluidic electricity generator) can be operated under various channel flow conditions conforming to flows found in daily life and in nature. In addtion, the IMIT(ITO mono-electrode based ionovoltaic transducer) generates electricity continuously and provides a clear understanding of the role of resistance in devices. In addition, we confirmed the effect of grain boundary and defect scattering effects on the device through the ITO mono-electrode fabricated by sputtering process modulation in various conditions. Especially, due to scale-up property, patternablitiy, and bendable characteristics means that this device can be used as various applications such as window or exterior of building and car. Also, theses structural study can be used not only for energy generating devices but also for various new types of sensors as shown in chapter5.

We believe that the structural engineering research of the device can produce a more optimized device through the advanced fabrication process, and that this study

will give us a better understanding of the electricity generation by the ionovoltaic device.

4.5 Experimental details

Fabrication of PDMS channel. A mold for the channel was used by combining PMMA blocks and PTFE tubes (DAEKWANG HIFLON). Two types of long tubes, 1.8 cm and 3.6 in length, with a 2.1 mm outside diameter were prepared for the channel. These tubes were inserted between PMMA blocks set a widths of 1.8 cm and 3.6 cm, respectively, and fixed with ketone tape. Then, unlinked 10:1 base and cross linker mixed PDMS (Sylgard-184, Dow Corning) solution was poured on the mold. This PDMS with mold was cured at 80 °C for 4 hours. After that, the PDMS and mold were detached, and inlet and outlet holes were drilled for tubing.

Materials and preparation of fluidic ionovoltaic device. In this experiment, the active transducer consisted of ITO glass, P4VP, and a silica gel layer. ITO glass was cut 1.8 cm by 4 cm, and 3.6 cm by 4 cm for the two types of channel lengths. P4VP solution 10 wt% was made with Poly (4-vinylphenol), Propylene glycol mono methyl ether acetate as the solvent and poly (melamine-co formaldehyde) methylated/ butylated as the cross linker (Sigma Aldrich) with a mass ratio 2:17:1. The silica gel film was formed by the sol-gel process. Silica sols were synthesized

with H2O, Ethanol, tetraethyl silicate (TEOS) (Sigma Aldrich) and 1H, 1H, 2H, 2H- Perfluorooctyl-triethoxysilane (POTS) (Sigma Aldrich) in acid conditions. A 0.031 mass ratio of TEOS and POTS was used in this experiment. The ITO glass was spin coated with the 10 wt% P4VP solution at 2000 rpm for 30 s and annealed at 200 °C for 15 min. Then, the two samples of P4VP coated ITO glass were exposed to ultraviolet ozone (100 mW/cm^2) for 30 min. Silica sol solution was spin coated with the same conditions as the P4VP. For the gelation of the silica sol layer, the substrate was baked at 200 °C. 99.4 degrees of contact angle were measured on the silica gel film, and this hydrophobic property of this film assisted in the dewetting process when the water flowed in the fluidic channel.

Performance measurement equipment. The voltage and current were measured with an oscilloscope (DPO-2024) and a pico-ammeter (Keithley Model 6485), respectively. The water and air were controlled with a syringe pump (KdScientific Inc.).

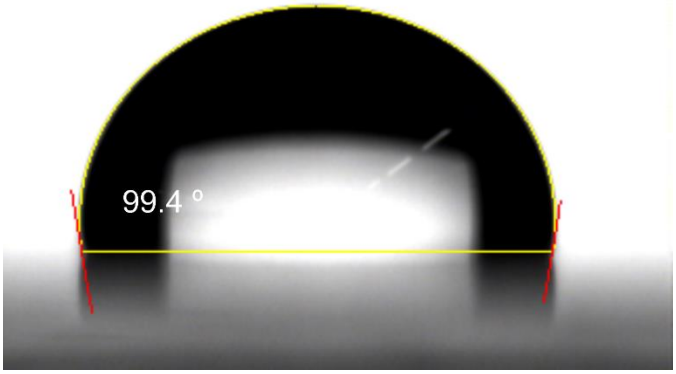

Figure 4. 12 A contact angle of 99.4 degrees was measured for a deionized water droplet on the silica gel film.

4.6 References

[1] Lee JW, Goulet MA, Kjeang E. Microfluidic redox battery. *Lab on a chip* **13**, 2504-2507 (2013).

[2] Figeys D, Pinto D. Lab-on-a-Chip: A Revolution in Biological and Medical Sciences. *Analytical Chemistry* **72**, 330 A-335 A (2000).

[3] Dittrich PS, Manz A. Lab-on-a-chip: microfluidics in drug discovery. *Nature reviews Drug discovery* **5**, 210-218 (2006).

[4] Rivet C, Lee H, Hirsch A, Hamilton S, Lu H. Microfluidics for medical diagnostics and biosensors. *Chemical Engineering Science* **66**, 1490-1507 (2011).

[5] Abou-Hassan A, Sandre O, Cabuil V. Microfluidics in inorganic chemistry. *Angewandte Chemie* **49**, 6268-6286 (2010).

[6] Borno RT, Steinmeyer JD, Maharbiz MM. Charge-pumping in a synthetic leaf for harvesting energy from evaporation-driven flows. *Applied Physics Letters* **95**, 013705 (2009).

[7] Yıldırım E, Külah H. Electrostatic energy harvesting by droplet-based multi-phase microfluidics. *Microfluidics and Nanofluidics* **13**, 107-111 (2012).

[8] Krupenkin T, Taylor JA. Reverse electrowetting as a new approach to high-power energy harvesting. *Nature communications* **2**, 448 (2011).

[9] van der Heyden F, Stein D, Dekker C. Streaming Currents in a Single Nanofluidic Channel. *Physical Review Letters* **95**, (2005).

[10] Mansouri A, Bhattacharjee S, Kostiuk L. High-power electrokinetic energy conversion in a glass microchannel array. *Lab on a chip* **12**, 4033-4036 (2012).

[11] Kwon S-H*, et al.* An effective energy harvesting method from a natural water motion active transducer. *Energy Environ Sci* **7**, 3279-3283 (2014).

[12] Park J, Yang Y, Kwon S-H, Kim YS. Influences of Surface and Ionic Properties on Electricity Generation of an Active Transducer Driven by Water Motion. *The Journal of Physical Chemistry Letters* **6**, 745-749 (2015).

[13] Yin J, Li X, Yu J, Zhang Z, Zhou J, Guo W. Generating electricity by moving a droplet of ionic liquid along graphene. *Nature nanotechnology* **9**, 378-383 (2014).

[14] Saisorn S, Wongwises S. Flow pattern, void fraction and pressure drop of two-phase air–water flow in a horizontal circular micro-channel.

Experimental Thermal and Fluid Science **32**, 748-760 (2008).

[15] Cabeza VS, Kuhn S, Kulkarni AA, Jensen KF. Size-controlled flow synthesis of gold nanoparticles using a segmented flow microfluidic platform. *Langmuir : the ACS journal of surfaces and colloids* **28**, 7007-7013 (2012).

[16] Miyabayashi K, Tonomura O, Hasebe S. Estimation of gas and liquid slug lengths for T-shaped microreactors. *Chemical Engineering Journal* **262**, 1137-1143 (2015).

[17] Aoki N, Tanigawa S, Mae K. A new index for precise design and advanced operation of mass transfer in slug flow. *Chemical Engineering Journal* **167**, 651-656 (2011).

[18] Nguyen N-T, Lassemono S, Chollet FA. Optical detection for droplet size control in microfluidic droplet-based analysis systems. *Sensors and Actuators B: Chemical* **117**, 431-436 (2006).

[19] Ide H, Kimura R, Kawaji M. Optical Measurement of Void Fraction and Bubble Size Distributions in a Microchannel. *Heat Transfer Engineering* **28**, 713-719 (2007).

[20] Burlage K, Gerhardy C, Praefke H, Liauw MA, Schomburg WK. Slug

length monitoring in liquid–liquid Taylor-flow integrated in a novel PVDF micro-channel. *Chemical Engineering Journal* **227**, 111-115 (2013).

[21] Dong T, Barbosa C. Capacitance Variation Induced by Microfluidic Two-Phase Flow across Insulated Interdigital Electrodes in Lab-On-Chip Devices. *Sensors* **15**, 2694-2708 (2015).

[22] Moon JK, Jeong J, Lee D, Pak HK. Electrical power generation by mechanically modulating electrical double layers. *Nature communications* **4**, 1487 (2013).

[23] Kong W*, et al.* Electret-based microfluidic power generator for harvesting vibrational energy by using ionic liquids. *Microfluidics and Nanofluidics*, (2014).

[24] Helseth LE, Guo XD. Contact Electrification and Energy Harvesting Using Periodically Contacted and Squeezed Water Droplets. *Langmuir : the ACS journal of surfaces and colloids*, (2015).

[25] Park, J. *et al.* Identification of Droplet-Flow-Induced Electric Energy on Electrolyte-Insulator-Semiconductor Structure. *J Am Chem Soc* **139**, 10968-10971 (2017).

[26] Kwon, S. H. *et al.* Fabric Active Transducer Stimulated by Water Motion

for Self Powered Wearable Device. *Acs Appl Mater Inter* **8**, 24579-24584 (2016).

[27] Yang, Y., Park, J., Kwon, S. H. & Kim, Y. S. Fluidic Active Transducer for Electricity Generation. *Sci Rep-Uk* **5** (2015).

[28] Yang, Y., Park, J., Yoon, S. G. & Kim, Y. S. Electricity modulation of a water motion active transducer via surface functionality control. *Nano Energy* **40**, 447-453 (2017).

[29] Park, J., Yang, Y., Kwon, S. H., Yoon, S. G. & Kim, Y. S. Analysis on characteristics of contact-area-dependent electric energy induced by ion sorption at solid-liquid interface. *Nano Energy* **42**, 257-261 (2017).

[30] Park, J., Yang, Y., Kwon, S. H. & Kim, Y. S. Influences of Surface and Ionic Properties on Electricity Generation of an Active Transducer Driven by Water Motion. *J Phys Chem Lett* **6**, 745-749 (2015).

[31] Moon, J. K., Jeong, J., Lee, D. & Pak, H. K. Electrical power generation by mechanically modulating electrical double layers. *Nat Commun* **4** (2013).

[32] Lin, Z. H., Cheng, G., Lee, S., Pradel, K. C. & Wang, Z. L. Harvesting Water Drop Energy by a Sequential Contact-Electrification and Electrostatic-Induction Process. *Adv Mater* **26**, 4690 (2014).

[33] Kwak, S. S. *et al.* Triboelectrification-Induced Large Electric Power Generation from a Single Moving Droplet on Graphene / Polytetra - fluoroethylene. *Acs Nano* **10**, 7297-7302 (2016).

[34] Yin, J. *et al.* Generating electricity by moving a droplet of ionic liquid along graphene. *Nat Nanotechnol* **9**, 378-383 (2014).

[35] Yin, J. *et al.* Waving potential in graphene. *Nano Energy 32, 125* (2017).

[36] T. Aviles et al., Recent developments in amorphous sputtered ITO thin films acting as transparent front contact layer of CIGS solar cells for energy autonomous wireless microsystems, 2011 37th *IEEE Photovoltaic Specialists Conference*, Seattle, WA, 2011, pp. 001235-001237.

[37] Kim, H. et al. Indium tin oxide thin films for organic light-emitting devices. *Appl Phys Lett* 74, 3444-3446 (1999).

[38] Kim, D. H., Park, M. R. & Lee, G. H. Preparation of high quality ITO films on a plastic substrate using RF magnetron sputtering. *Surf Coat Tech* 201, 927-931 (2006).

[39] Wu, W. F. & Chiou, B. S. Effect of oxygen concentration in the sputtering ambient on the microstructure, electrical and optical properties of radio-frequency magnetron-sputtered indium tin oxide films. *Semicond Sci Tech*

11, 196-202 (1996).

[40] Lee, K. H., Jang, H. W., Kim, K.-B., Tak, Y.-H. & Lee, J.-L. Mechanism for the increase of indium-tin-oxide work function by O2 inductively coupled plasma treatment. *Journal of Applied Physics* 95, 586-590, doi:10.1063/1.1633351 (2004).

Chapter. 5 Conclusion

I have improved the ionovoltaic device and explored for more accurate understanding of electricity generation phenomenon in the device through the surface modification and structural engineering. This study suggests various possibilities of ionovoltaic device research and dramatically improves the uniform surface material and device structure which prevented the exploration of the cause of the electricity generation and the wide range of applications.

Using APTES and PFOTS, the hydrophobic surface with positive surface potential was introduced into an ionovoltaic device and the charge reversal effect on the device was confirmed for the first time. The pH-sensitive nature of the device's surface has also demonstrated its potential for use as various active sensor based on aqueous such as pH sensor and urea sensor (chapter 2, 3).

By studying the structural engineering, we have devised a device that can be driven in various environments, especially in the micro fluidic channels. In addition, through the study of the electrodes, we could understand the movement of the electrons more clearly and the effect of the electrode resistance on the performance of the ionovoltaic device. Structural engineering studies have dramatically increased the generation time of electricity, which is positive in

terms of increasing energy density, suggesting that it can be used as an energy harvester (chapter 4).

This study implies extensibility of surface treatment and provides clues as to the role of electrodes in the development of ionovoltaic devices. Therefore, I believe that this work can be a key to the research as utilization of various sensors and the optimization of energy harvesting device. Finally, the advantages and disadvantages of my research results and future research directions can be summarized as follows.

■ Advantages

Surface modification.

-. Simple step method to make a positive surface with hydrophobicity.

-. Easy to change enzyme attached to the bar; Utilizing the LBL method.

-. Eco-friendly, low-cost, simple fabrication method, easy modification of functional groups.

Structural Engineering.

-. Stable reliability of operation: amorphouse phase of the insulator films enhances reliability of the operation for the device.

-. Simple engineering for controlling the resistance of the electrode.

■ Disadvantages

Surface modification.

-. Need of hydrophobic properties.

-. Stability, reusability issues.

Structural engineering

-. Difficulty in evaluating the characteristics in the subdivided conditions.

-. Lack of theoretical approach in detail.

■ Future research direction

-. A clear understanding of the effects of cations and anions.

-. Studies on the effects on multivalent ions.

-. Selectivity of ions in a device.

-. Developlment of various fabrication methods for making optimized devices.

-. More electricity production.

-. Electrical signal generation in steady state in contact with water.

List of publications

-. **YoungJun Yang**, Junwoo Park, Sun Geun Yoon, and Youn Sang Kim, ″Electricity modulation of a water motion active transducer via surface functionality control″ Nano Energy, 40, 447 (2017)

-. **YoungJun Yang**, Junwoo Park, Soon-Hyung Kwon, and Youn Sang Kim, ″Fluidic Active Transducer for electricity generation″ Scientific Reports, 5, 15695 (2015)

-. Sun Geun Yoon, **YoungJun Yang**, Huding Jin, Won Hyung Lee, Ahrum Sohn Sang-Woo Kim, Junwoo Park and Youn Sang Kim, "A Surface-Functionalized Ionovoltaic Device for Probing Ion-Specific Adsorption at the Solid–Liquid Interface", Advanced Materials, 1806268, (2018)

-. Junwoo Park, Suhwan Song, ChaeHo Shin, **YoungJun Yang**, Stefan A. L. Weber, Eunji Sim, Youn Sang Kim, ″Ion specificity on electric energy generated by flowing water droplets″ Angewandte Chemie International Edition, 57, 2091 (2018)

-. Junwoo Park, **YoungJun Yang**, Soon-Hyung Kwon, Sun Geun Yoon, and Youn Sang Kim, ″Analysis on characteristics of contact-area-dependent electric energy induced by ion sorption at solid-liquid interface″ Nano Energy, 42, 257 (2017)

-. Junwoo Park, Suhwan Song, **YoungJun Yang**, Soon-Hyung Kwon, Eunji Sim, and Youn Sang Kim, ″Identification of droplet-flow-induced electric energy on electrolyte−insulator−semiconductor structure″ Journal of The American Chemical Society, 139, 10968-10971 (2017)

-. Soon-Hyung Kwon, Won Keun Kim, Junwoo Park, **YoungJun Yang**, Byungwook Yoo, Chul Jong Han, and Youn Sang Kim, ″ Fabric active transducer stimulated by water motion for self-powered wearable device″ ACS Appl. Mater. Interfaces, 8, 24579-24584 (2016)

-. Junwoo Park, **YoungJun Yang**, Soon-Hyung Kwon, and Youn Sang Kim, ″Influences of surface and ionic properties on electricity generation of an active transducer driven by water motion″ The Journal of Physical Chemistry Letters, 6, 745−749 (2015)

-. Soon-Hyung Kwon, Junwoo Park, Won Keun Kim, **YoungJun Yang**, Eungkyu Lee, Chul Jong Han, Si Yun Park, Jeongno Lee and Youn Sang Kim, ″An effective energy harvesting method from a natural water motion active transducer″ Energy & Environmental Science, 7, 3279-3283 (2014)

요 약 (국문초록)

에너지 수확과 센서 활용을 위한 ionovoltaic 장치의 표면 개질과 구조 공정에 관한 연구

양 영 준
융합과학부 나노융합과
융합과학기술대학원
서울대학교

최근 Ionovoltaic 변환기라 명명된, 액체와 고체 표면의 접촉에서 전기가 발생하는 현상을 이용한 전기 변환 장치에 관한 연구가 많은 관심을 받고 있다. 신재생 친환경 에너지 발전 장치에 관한 필요성이 커지고 수용액 기반에서 능동적으로 작동 할 수 있는 다양한 센서에 관한 요구가 꾸준히 증가하는 가운데, ionovoltaic 소자는 이러한 요구를 충족 시킬 수 있는 능동형 장치로서 주목받고 있다. 하지만 ionovoltaic 소자를 에너지 발전 소자와 능동적 센서로 실질적 활용과 적용을 하기에는 출력 에너지 밀도가 낮고, 공정이 복잡하다. 더욱이 충분히 밝혀지지 않은 소자의 구동 원

리와 소자의 획일적인 재료 및 구조 연구는 소자의 다양한 활용 발전을 가로막고 있다. 여기, 이 학위 연구는 ionovoltaic 장치의 (i) 표면 개질과 (ii) 구조 공정 개선, 두 가지 연구를 통해 계면에서의 이온거동에 의한 전기 발생 현상을 보다 명확히 밝히며 이를 통해 센서와 에너지 수확 장치로서의 폭 넓은 활용을 다룬다.

첫째, 기존에 사용되었던 불소 기반의 획일적인 소수성 표면 물질을 벗어나 표면 개질을 통한 새로운 전기적 특성을 갖는 소수성 표면 공정을 ionovoltaic 전환 소자에 적용하여 액체와 고체 계면에서의 이온 거동을 이용한 다양한 센싱 어플리케이션에 적용하였다. 음의 표면전위를 갖는 소수성 표면의 변환기와 양의 표면전위를 갖는 소수성 표면의 변환기를 개발하여 비교 분석 하였으며 이온 거동에 의한 전기신호 반전 효과를 처음으로 확인 하였다. 뿐만 아니라, 산, 염기에 민감한 표면 특성을 활용하여 pH 센서 및 요소(urea) 센서로서 활용성을 검증하였다.

둘째, 기존에 사용되었던 2 전극 시스템의 획일적인 소자의 구조를 탈피하고 새로운 형태의 소자 구조 공정을 통해 액체와 고체 표면의 접촉이 전기신호로 변환되는 원리 파악과 센싱 및 에너지 수확장치로서의 적용 가능성을 제시하였다. 소자의 전체적인 구조 공정과 전극 연구를 통해서 전기 신호의 발생 지속시간을 조절 할 수 있었으며 에너지밀도를 높일 수 있었다. 뿐만 아니라 투명하면서도 전기를 발생시킬 수 있는 고저항 ITO

전극 개발을 통해 건물이나 자동차의 외관 및 창문에 활용 될 수 있는 에너지 수확장치를 개발하여 ionovoltaic 장치의 폭넓은 활용가능성을 제시하였다.

주요어: Ionovoltaic 장치, 에너지 전환 소자, 고체-액체계면, 표면처리, 센서

학 번: 2013-23749